

Measurement of OH, H₂SO₄, MSA, and HNO₃ Aboard the P-3B Aircraft

NASA Contract No.: NCC-1-421
Georgia Tech Project No. G-35-663

FINAL Report

July 1, 2000 – June 30, 2003

Submitted to:

NASA Langley Research Center
Mail Stop
Hampton, VA 23681-2199

Attn: Victor Delnore

Submitted by:

School of Earth and Atmospheric Sciences
Georgia Institute of Technology
Atlanta, GA 30332

Principal Investigator: F. L. Eisele

Performance Report

Work on this project began in the summer of 2000 with some upgrades to the 4-channel mass spectrometer instrument used on TRACE-P. The standard quadrupole mass spectrometer unit used previously to measure OH was replaced with a new quadrupole unit with pre and post filters. This improved the throughput of the OH mass spectrometer channel by nearly a factor of 2, thus increasing the measurement sensitivity for OH, H₂SO₄ and MSA by about 30% (or the square root of the ion signal gain). Several modifications were also made to the nitric acid channel as well. The ion source geometry was modified, resulting in higher reactant ion concentrations. The method for adding reactant ion source compounds (in this case MSA) was improved so that the ion source was not over-saturated with MSA between flights. Inlet and calibration gas injection were also modified. Much time was spent calibrating the HNO₃ portion of the instrument and looking for potential interferences, since the ion source geometry and ion chemistry used on TRACE-P had not been flown previously. The new HNO₃ measurement technique appeared to work well, even at reduced inlet temperatures used to simulate flight conditions. The OH/H₂SO₄/MSA portion of the instrument was also retested before shipment into the field and also appeared to function properly. The instrument and associated supplies and backups were packed up in December 2000 and shipped to the NASA Wallops Island Facility in early January 2001. The instrument was installed on the NASA P-3 in January and was tested on the ground until mid-February, when test flights began. The OH, H₂SO₄, and MSA measurements functioned well, while new problems with the HNO₃ measurement were encountered during flight tests. Many of the problems were related to calibration and background measurements, which was not totally unexpected. In our TRACE-P proposal, we proposed absolute measurements of OH, H₂SO₄ and MSA but only relative measurements of HNO₃ because of problems encountered on a previous NCAR flight mission. The instrument used on that mission was an older version of that used of TRACE-P, but had many similarities. Fortunately, as the mission progressed the calibration and background problems were largely solved, and not only relative but also absolute measurements of HNO₃ were made. This was a major step beyond what was proposed, and was largely made possible by many hours of flight testing.

TRACE-P ended in April of 2001 and our instrument was off-loaded and shipped back to the laboratory by May. Therefore, the second year's efforts began with data analysis and laboratory calibrations and testing. There are over 50 gas flow or electric field parameters which are measured every few seconds along with our measurements to insure proper instrument operation. One of the first data analysis tasks was thus to sort all of the measurement data, and reject any measurements taken when flow or electric field conditions were out of range because of some type of instrument failure. A second task was to recheck field calibration results, to do laboratory calibration of our UV diodes used to measure photon fluxes in the OH and H₂SO₄ calibration sources, and to carry out nitric acid permeation cell calibrations. Diode calibrations turned up a discrepancy which took many weeks to resolve, and resulted in a significant change in our final data, particularly at higher altitudes. There was a leak that developed in part of our OH calibration system which caused an attenuation of the UV photon beam used for the in flight OH calibration. Fortunately, due to redundant measurements of this flux, the error could be detected. Laboratory simulations of the problem after TRACE-P showed that about a 7-cm path length of the optical path thought to be filled with nitrogen was actually filled with air at ambient pressure and humidity. This happened after the test flights but just before the beginning of the mission. Correcting the UV flux for the absorption by the additional ambient O₂ and H₂O concentration then gave good agreement between the 2 different diode readings. This altitude dependent correction was then applied to the OH, H₂SO₄, and MSA data and the results were submitted to the data archive. This whole process took several additional months.

The nitric acid data calibration tests were much more straightforward. Permeation cell weighings were performed for several months following the mission to redetermine emission rates. Also, the dilution of calibration gas in the inlet tube had to be rechecked before final data was submitted. All 4 compounds were measured successfully with good sensitivity, accuracy, and temporal coverage and all were submitted to the TRACE-P data archive. Even beyond this submission, however, continued efforts to improve the OH calibration scheme were undertaken, through the purchase of a new type of standard NIST UV calibration diode and the construction and testing of a more portable calibration apparatus. This both provided increased confidence in previous

measurements and will provide a new in field diode calibration capability for future studies.

After data submission to the TRACE-P archive, the more complex data analysis phase began, trying to compare our data with other measured and modeled results. As part of this process, particularly interesting events are also separated out for more detailed analysis. One particularly interesting event occurred during a nighttime flight out of Midway Island. Hydroxyl radical concentrations were essentially zero at all altitudes, while sulfuric and methane sulfonic acid concentrations were quite substantial, particularly in the boundary layer (see Figures 1 and 2). Since gas phase sulfuric acid is

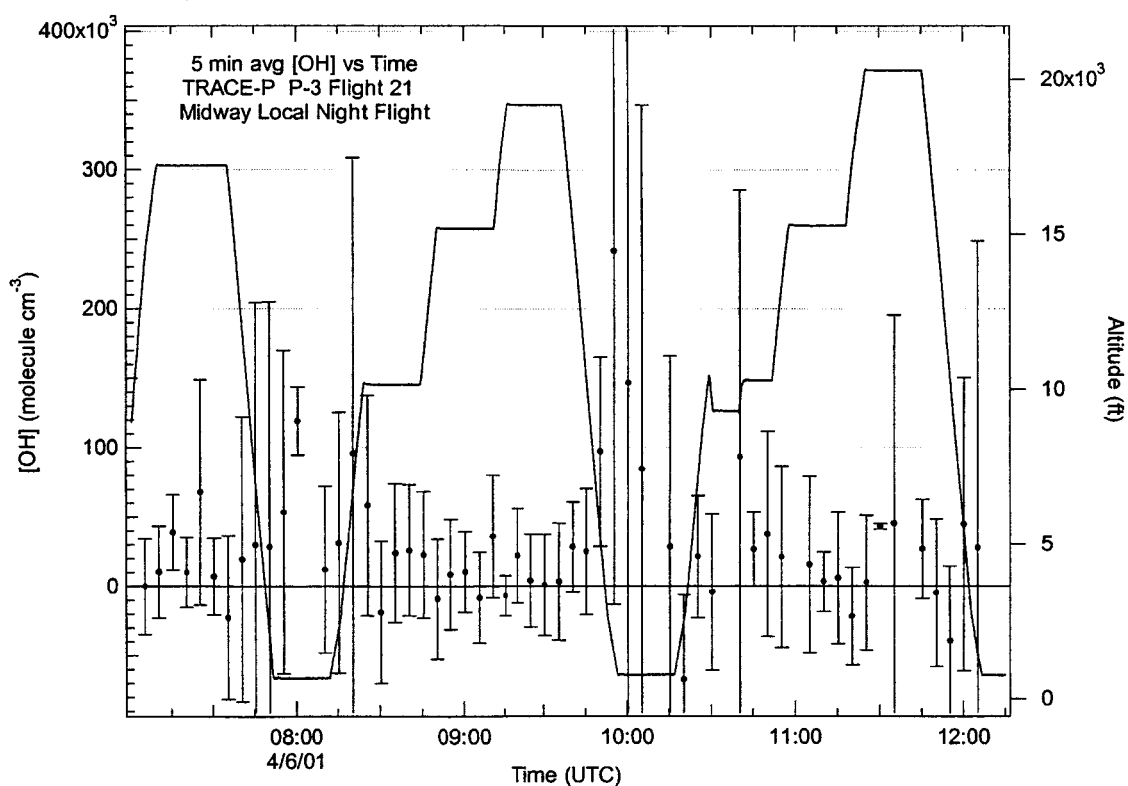


Figure 1. Five minute averaged OH measurements and 2σ error bars for a night flight near Midway Island. Note that except for a few instances when exceptional high nighttime H_2SO_4 was observed the 2σ error bars for OH are well below $\pm 1 \times 10^5$ molecules cm^{-3} and not uncommonly $\pm 3-5 \times 10^4$ molecules cm^{-3} .

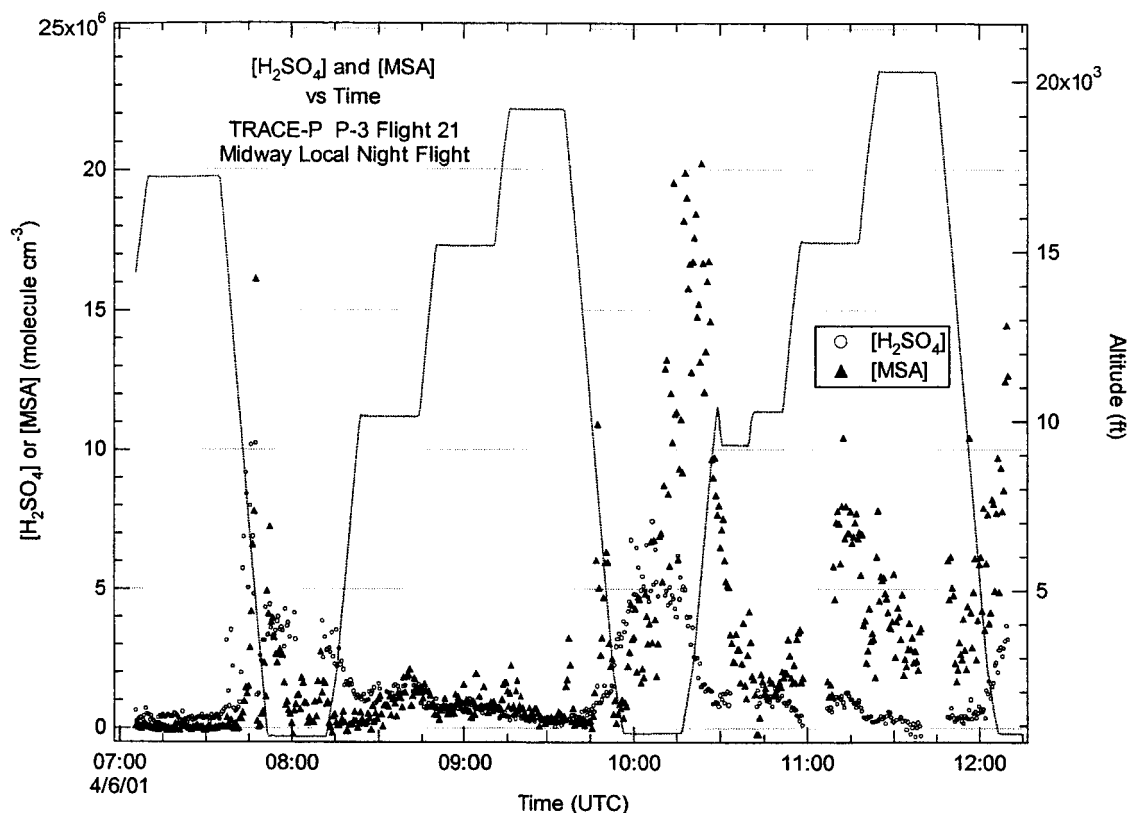


Figure 2. Sulfuric and methane sulfonic acid observed at night and in some cases well above the boundary layer near Midway Island.

typically formed by OH initiated oxidation of SO_2 , at night, in the absence of OH, H_2SO_4 concentrations are normally in the low 10^5 molecules cm^{-3} range or less, due to its loss onto particles. In the boundary layer, typically containing high particle surface area and higher relative humidity, H_2SO_4 lifetimes should be $\leq 10^3$ seconds and it should be nearly completely lost to particles (vapor pressure $< 10^5$ molecules cm^{-3}). The observed boundary layer concentrations of H_2SO_4 up to about 5×10^6 molecules cm^{-3} strongly suggest that a previously unknown nighttime source exists for this compound, presumably an oxidant capable of converting reactive sulfur gases such as SO_2 or DMS into H_2SO_4 . A similar situation exists for MSA. While MSA is more volatile than H_2SO_4 , we have not seen evidence of its leaving particles at relative humidities above about 20%, and certainly not under typical marine boundary layer conditions. Therefore the presence of gas phase MSA at night also suggests the presence of an unknown nighttime oxidant to convert DMS into MSA. Reactions with NO_3 could provide such an

oxidation mechanism, except that NO_x was very low in this remote marine environment. Interestingly, MSA concentrations are in several instances seen to be much higher than H_2SO_4 concentrations, which is very atypical of OH induced oxidation at the latitude/temperatures of Midway Island. If a single oxidant is responsible for generating both gas phase H_2SO_4 and MSA it apparently reacts with SO_2 and DMS at a very different rate than does OH.

Some of the highest sulfuric acid concentrations observed were also recorded during TRACE-P. Sulfuric acid reached concentrations greater than 2×10^8 molecules cm^{-3} in relatively low altitude plumes during the P-3b flight number 17 as shown in Figure 3. These high concentrations can lead to aerosol nucleation and rapid

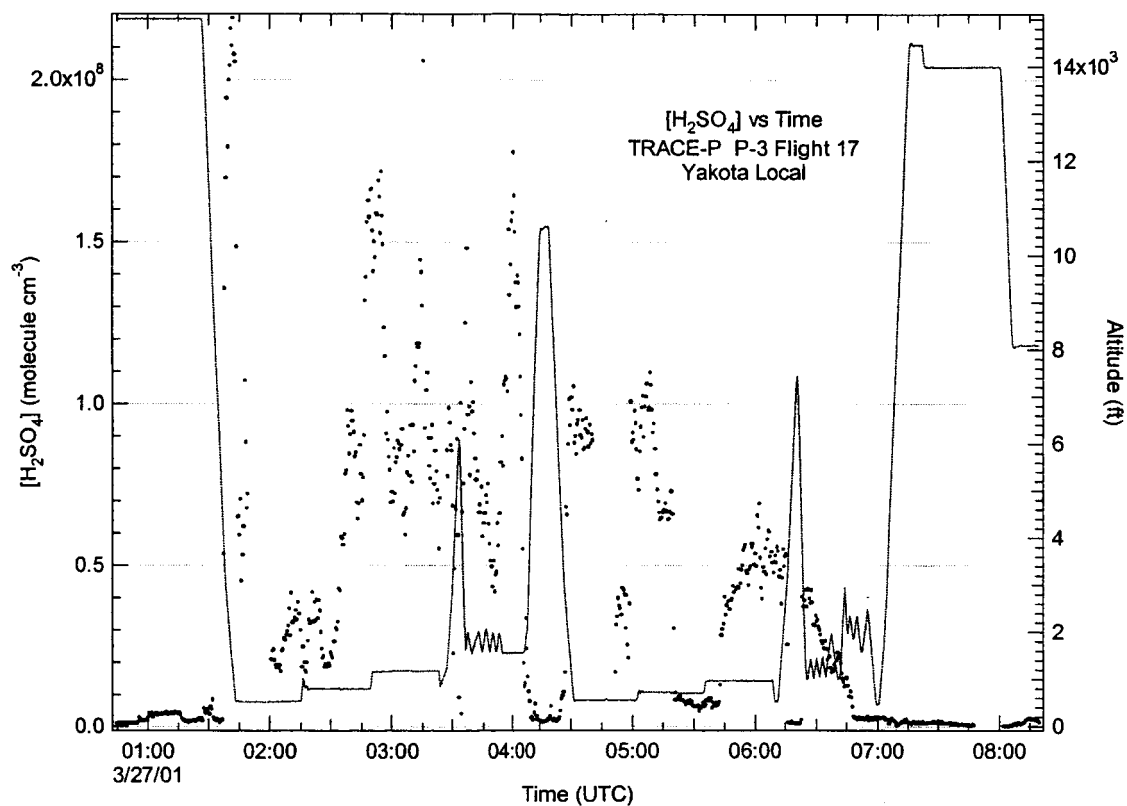


Figure 3. Some of the highest sulfuric acid observed in a NASA flight mission occurred in relatively low altitude plumes near Japan. These are the conditions that can lead to rapid aerosol nucleation and growth.

particle growth, which in turn can alter cloud properties, heterogeneous chemistry etc. Such results are discussed in far more detail in a manuscript by Mauldin et al. to be published in the first special TRACE-P issues (see Appendix A). The results of our nitric acid measurements are in press and will also appear in the first TRACE-P special issues. These results are included in Appendix B.

In addition to improving our understanding of Asian outflow and its processing as it transits the Pacific, TRACE-P also provided an opportunity to intercompare measurement results from the NASA P-3B and DC-8 aircraft. The results of both our measurements as well as those from many other instruments on both aircraft are discussed in detail in a manuscript by Eisele et al. to be published in the first special TRACE-P issue. Both our OH and HNO₃ measurements generally agreed with DC-8 measurements of the same compound within the stated error limits. Our H₂SO₄ and MSA measurements could not be intercompared because they are the only measurements of these compounds made on TRACE-P. Additional details of our OH and HNO₃ measurements can be found in Appendix A and B respectively. In addition to the papers listed in Appendix A-B and the measurement intercomparison paper which were submitted by our group we have also co-authored many other TRACE-P papers and presentations which are listed on the next few pages.

Papers resulting from our TRACE-P measurements.

1. The Spatial Distribution and Size Evolution of Particles in Asian Outflow: The Significance of Primary and Secondary Aerosols During ACE-Asia and TRACE-P, C. McNaughton, S. Howell, A. Clarke, K. Moore, R. Weber, K. Meier, T. Anderson, S. Masonic, D. Covert, G. Buzorius, F. Brechtel, F. Eisele, L. Mauldin, A. Bandy and B. Blomquist (submitted to Journal of Geophysical Research).
2. Highlights of OH, H₂SO₄, and MSA Measurements Made Aboard the NASA P-3B During TRACE-P, R. Mauldin III, C. Cantrell, M. Zondlo, E. Kosciuch, F. Eisele, G. Chen, D. Davis and R. Weber. Journal of Geophysical Research, in press.
3. Summary of Measurement Intercomparisons During TRACE-P, F. L. Eisele, L. Mauldin, C. Cantrell, M. Zondlo, E. Apel, A. Fried, J. Walega, R. Shetter, B. Lefer, F. Flocke, A. Weinheimer, M. Avery, S. Vay, G. Sachse, H. B. Singh, W. Brune, H. Harder, M. Martinez, A. Bandy, D. Thornton, B. Heikes, Y. Kondo, D. Riemer, S. Sandholm, D. Tan, R. Talbot and J. Dibb. Journal of Geophysical Research, in press.
4. Regional-Scale Chemical Transport Modeling in Support of the Analysis of Observations Obtained During the TRACE-P Experiment, G. Carmichael, Y. Tang, G. Kurata, I. Uno, D. Streets, J-H. Woo, H. Huang, J. Yienger, B. Lefer, R. Shetter, D. Blake, E. Atlas, A. Fried, E. Apel, F. Eisele, C. Cantrell, M. Avery, J. Barrick, G. Sachse, W. Brune, S. Sandholm, Y. Kondo, H. Singh, R. Talbot, A. Bandy, D. Thornton, A. Clarke and B. Heikes. Journal of Geophysical Research, in press.
5. The Characteristics and Influence of Biomass Burning Aerosols on Fine Particle Ionic Composition Measured in Asian Outflow During TRACE-P, Y. Ma, R. Weber, Y-N. Lee, D. Thornton, A. Bandy, A. Clarke, D. Blake, G. Sachse, H. Fuelberg, C. Kiley, J-H. Woo, D. Streets, G. Carmichael and F. Eisele. Journal of Geophysical Research, in press.
6. Peroxy Radical Behavior During TRACE-P as Measured Aboard the NASA P-3B Aircraft, C. Cantrell, G. Edwards, S. Stephens, R. Mauldin, M. Zondlo, E. Kosciuch, F. Eisele, R. Shetter, B. Lefer, S. Hall, F. Flocke, A. Weinheimer, A. Fried, E. Apel, Y. Kondo, D. Blake, N. Blake, I. Simpson, A. Bandy, D. Thornton, B. Heikes, H. Singh, W. Brune, H. Harder, M. Martinez-Harder, D. Jacob, M. Avery, J. Barrick, G. Sachse, J. Olsen, J. Crawford and A. Clarke. Journal of Geophysical Research, in press.
7. Development and Characterization of an Airborne-Based Instrument Used to Measure Nitric Acid During the NASA TRACE-P Field Experiment, M. Zondlo, R. Mauldin, E. Kosciuch, C. Cantrell and F. Eisele. Journal of Geophysical Research, in press.
8. New Particle Formation in Anthropogenic Plumes Advecting From Asia Observed During TRACE-P, R. Weber, S. Lee, G. Chen, B. Wang, V. Kapustin, K. Moore, A. Clarke, L. Mauldin, E. Kosciuch, C. Cantrell, F.

- Eisele, D. Thornton, A. Bandy, G. Sachse and H. Fuelberg. *Journal of Geophysical Research*, in press.
9. Clouds and Trace Gas Distributions During TRACE-P, J. Crawford, J. Olson, D. Davis, G. Chen, J. Barrick, R. Shetter, B. Lefer, C. Jordan, B. Anderson, A. Clarke, G. Sachse, D. Blake, H. Singh, S. Sandolm, D. Tan, Y. Kondo, M. Avery, F. Flocke, F. Eisele, L. Mauldin, M. Zondlo, W. Brune, H. Harder, M. Martinez, R. Talbot, A. Bandy, D. Thornton and S. Vay. *Journal of Geophysical Research*, in press.
 10. Synoptic-Scale Transport of Reactive Nitrogen Over the Western Pacific in Spring, Y. Miyazaki, Y. Kondo, M. Koike, K. Kita, N. Takegawa, H. Fuelberg, G. Sachse, F. Flocke, A. Weinheimer, H. Singh, F. Eisele, M. Zondlo, R. Talbot, S. Sandholm, M. Avery and D. Blake. *Journal Geophysical Research*, in press.
 11. Export of Anthropogenic Reactive Nitrogen and Sulfur Compounds from the East Asia Region in Spring, M. Koike, Y. Kondo, K. Kita, N. Takegawa, Y. Masui, Y. Miyazaki, M. Ko, R. Weber, D. Thornton, G. Sachse, S. Vay, D. Blake, D. Streets, F. Flocke, A. Weinheimer, F. Eisele, S. Sandholm, H. Singh and R. Talbot. *Journal of Atmospheric Chemistry*, in press.

Presentations resulting from our TRACE-P measurements

American Geophysical Union, Fall Meeting, San Francisco, CA, December 6-10, 2002

1. F. L. Eisele, et al., Informal Instrument Intercomparison.
2. J. Olson, et al., Testing Fast Photochemical Theory During TRACE-P Based on Measurements of OH, HO₂, NO₂, and CH₂O. Poster
3. A. Hamlin, et al., Chemical Evolution of Ozone and its Precursors in Asian Pacific Rim Outflow During TRACE-P. Poster
4. L. Mauldin, C. Cantrell, M. Zondlo, E. Kosciuch, F. Eisele, R. Weber, D. Thornton, A. Bandy and D. Blake, Evidence of Nighttime Oxidation in the Remote Pacific Boundary Layer During the NASA TRACE-P Study. Poster
5. F. Flocke, et al., Observation of PANs on Board the NASA P-3 During TRACE-P. Poster
6. J. H. Crawford, et al., Clouds and Trace Gas Trends Observed During TRACE-P. Poster
7. G. Huey, et al., Measurements of Nitric and Pernitric Acids at the South Pole During ISCAT 2000. Invited
8. M. A. Zondlo, R. L. Mauldin, E. K. Kosciuch, C. A. Cantrell and F. L. Eisele, Influence of Asian Outflow on the Tropospheric Distribution and Lifetime of Nitric Acid Over the Western and Central Pacific. Poster
9. K. Kita, et al., Sources, Distribution and Partitioning of Reactive Nitrogen in the Lower Troposphere Over Western Pacific During TRACE-P. Poster
10. Cantrell, et al., Peroxy Radical Measurements Aboard the NASA P-3B During TRACE-P. Poster
11. G. D. Edwards, C. A. Cantrell, S. Stephens, R. E. Shetter, L. Mauldin, E. Kosciuch, D. J. Tanner and F. L. Eisele, A Chemical Ionisation Mass Spectrometer Instrument for the Measurement of Tropospheric HO₂ and RO₂. Poster
12. C. S. McNaughton, S. G. Howell, A. D. Clarke, B. Blomquist, T. Anderson, S. J. Masonis, R. J. Weber, F. L. Eisele and L. Mauldin, The Spatial Distribution and Size Evolution of Particles in Asian Outflow: The Significance of Primary and Secondary Aerosol During ACE-ASIA and TRACE-P. Poster

American Geophysical Union, Fall Meeting, San Francisco, CA, December 10-14, 2001

1. M. A. Zondlo, R. Mauldin, C. Cantrell, E. Kosciuch and F. Eisele, Measurements of Nitric Acid Over the Western Pacific From a New Airborne Instrument.

Appendix A: Highlights of OH, H₂SO₄, and MSA Measurements Made Aboard the NASA P-3B During TRACE-P, Mauldin et al.

Appendix B: Development and Characterization of an Airborne-Based Instrument used to measure Nitric Acid During the NASA TRACE-P Field Experiment, Zondlo et al.

Highlights of OH, H₂SO₄, and MSA Measurements Made Aboard the NASA P-3B During TRACE-P

**R.L. Mauldin III¹, C.A. Cantrell¹, M. Zondlo^{1,3}, E. Kosciuch¹, F.L. Eisele^{1,2},
G. Chen^{2,4}, D. Davis², and R. Weber²
J. Crawford⁴, D. Blake⁵, A. Bandy⁶, and D. Thornton⁶**

- 1. Atmospheric Chemistry Division, National Center for Atmospheric Research, Boulder, Colorado**
- 2. School of Earth and Atmospheric Sciences, Georgia Institute of Technology, Atlanta, GA**
- 3. Now at Southwest Sciences Inc., Santa Fe, NM**
- 4. NASA Langley Research Center, Hampton, VA**
- 5. Department of Chemistry, University of California, Irvine, Irvine, CA**
- 6. Department of Chemistry, Drexel University, Philadelphia, PA**

Abstract

Measurements of hydroxyl radical (OH), sulfuric acid (H_2SO_4), and methane sulfonic acid (MSA) were performed aboard the NASA P-3B using the Selected Ion Chemical Ionization Mass Spectrometry technique during the TRansport And Chemical Evolution – Pacific (TRACE-P) study. Photochemical box model calculations of OH concentrations yielded generally good agreement with an overall tendency to overestimate the measured OH by ~20%. Further analysis reveals that this overestimation is present only at altitudes greater than ~1.5 km, with the model underestimating OH measurements at lower altitudes. Boundary layer H_2SO_4 measurements, performed in a volcanic plume off the southern coast of Japan, revealed some of the largest marine boundary layer H_2SO_4 concentrations ever observed, and were accompanied by new particle formation. Nighttime measurements of OH, H_2SO_4 , and MSA in the remote pacific off Midway Island, revealed significant boundary layer concentrations of H_2SO_4 , and MSA, indicating evidence of nighttime boundary layer oxidation processes, but in the absence of OH. A cursory exploration of the sources of production of the H_2SO_4 and MSA observed at night is presented.

1. Introduction

The NASA Global Tropospheric Experiment (GTE) TRANsport and Chemical Evolution over the Pacific (TRACE-P) study offered a unique opportunity to perform OH, H₂SO₄, and Methane Sulfonic Acid (MSA) measurements over a wide variety of environments and conditions. Regions of Asian outflow could produce air masses perturbed with high levels NO_x, SO₂, CO, CH₄ and numerous other hydrocarbons.

In these regions the hydroxyl radical (OH) will be one of the primary cleansing or oxidizing agents, significantly controlling the chemical evolution of air masses during transport. Through multi-step reactions, OH is responsible for the removal of most atmospheric carbon containing compounds (CO, CH₄, NMHC's), either anthropogenic or biogenic in origin, and their subsequent oxidation products. These reactions ultimately lead to the formation of H₂O and CO₂. The lifetime of these organic species is determined in large part by the concentration of OH. Thus, in part, OH controls how carbon is partitioned between the product CO₂ and organic emissions like CH₄ and intermediates such as CO (also a direct emission) at any given time after reactive carbon enters the atmosphere.

H₂SO₄ is produced by the OH initiated oxidation of SO₂. Natural sources of SO₂ include oxidation of reduced sulfur (DMS) emitted by the ocean and direct volcanic emission. Large quantities of SO₂ are also produced on the Asian continent from the use of high sulfur coal as a fuel source. Once in the atmosphere, much of this SO₂ is oxidized by OH to ultimately form H₂SO₄. Once formed, gas phase H₂SO₄ plays an important role in governing the rate of new particle formation and particle growth rates and ultimately cloud condensation nucleus (CCN) production and cloud properties. The aerosols and CCN produced by these nucleation and growth processes govern visibility reduction and climate modification [Charlson *et al.*, 1987; Twomey *et al.*, 1984].

In the remote marine environment, MSA is produced via the oxidation of DMS [Davis *et al.*, 1998]. Once in the atmosphere, DMS is oxidized by OH via a branched mechanism to produce either SO₂, much of which eventually forms H₂SO₄, or products which can lead to the formation of MSA, [Ayers *et al.*, 1991; Yin *et al.*, 1990; Toon *et al.*, 1987; Hataleyama *et al.*, 1982]. Once formed, gas phase MSA has a lifetime similar to that of H₂SO₄, being lost to surfaces or rainout [Ayers *et al.*, 1991; Yin *et al.*, 1990]. Recent results from the Tropospheric Ozone Production about the Spring Equinox (TOPSE) study have shown MSA to be present in air masses with anthropogenic influences [Mauldin *et al.*, 2003].

Here we present highlights of OH, H₂SO₄, and MSA measurements made aboard the NASA P-3B during the TRACE-P study. Overall model comparisons will be discussed. H₂SO₄ data from a flight through a volcanic plume off the southern coast of Japan will be presented. Additionally, some very interesting results from a night time flight out of Midway Island will be presented.

2. Data Acquisition and Analysis

Measurements of OH, H₂SO₄, and MSA were performed aboard the NASA P-3B using the Selected Ion Chemical Ionization Mass Spectroscopy, SICIMS, technique. A schematic diagram of the instrument used in this study can be found in Figure 1. The system consists of three major sections: a shrouded inlet which straightens and slows the air flow; an ion reaction region in which the chemical ionization reactions occur; and a turbo molecular pumped vacuum chamber which houses a quadrupole mass spectrometer and an electron multiplier detector. The measurement technique and system used in this study have been described in detail elsewhere [Eisele and Tanner, 1991; Eisele and Tanner, 1993, Tanner *et al.*, 1997; Mauldin *et al.*, 1998; Mauldin *et al.*, 1999]; therefore the reader is directed to those works for experimental details.

The same calibration assembly and technique as described in *Mauldin et al.* [2001] were employed in the measurements presented here. Briefly, the technique involves the photolysis of H₂O at 184.9 nm to produce a known amount of OH in front of the 1.9 cm curved sampling inlet. As shown in Figure 1, light from a Pen Ray Hg lamp passes through a cylindrical lens (Suprasil), reflects off of two mirrors coated to selectively reflect 184.9 nm, and then exits the calibration assembly via a Suprasil window and shutter/slit mechanism. The light then passes through an enclosed 2.5 cm path before illuminating the sample flow. To prevent light absorption and the build up of O₃ within the calibration assembly, the calibration housing was purged with N₂. As OH is converted to, and measured as H₂³⁴SO₄, this calibration also serves as a calibration for ambient H₂SO₄, and MSA [*Eisele and Tanner*, 1991].

The OH concentration produced by the calibration source is a function of the intensity of the photon flux at 184.9 nm, the [H₂O], the absorption cross-section at 184.9 nm, the yield of OH from H₂O photolysis, and the sample flow velocity. The flow velocity was measured using a Pitot tube mounted just forward of the 1.9 cm curved inlet, and the [H₂O] was measured using a dew point hygrometer aboard the aircraft. To determine the photon flux from the lamp at 184.9 nm, vacuum UV photo diodes mounted on an x/y traverse were used to periodically map out the light field on the ground. The quantum efficiency of these diodes were compared to a National Institute of Standards and Technologies (NIST) standard diode both prior to and after the mission. A value of 7.14×10^{-20} cm² molecule was used for the H₂O absorption cross section at 184.9 nm [*Cantrell et al.*, 1997].

Problems arose with the implementation of this technique. Prior to deployment, a leak developed between the Suprasil window and the calibration housing allowing ambient air to enter the housing. Unfortunately, this leak was not detected until after the study. Briefly stated this leak caused the following problem. Normally the photon fluence at 184.9 nm is determined from diode

mappings performed in front of the 1.9 cm curved inlet while the plane is on the ground. The light exiting the lamp assembly is then calculated by increasing the mapping values to account for absorption due to ambient O₂ and H₂O over the 7.26 cm path to the curved inlet. For in situ calibrations, the photon fluence at the 1.9 cm curved inlet is calculated by decreasing the flux value at the lamp exit to account for absorption due to ambient O₂ and H₂O over the 7.26 cm path to the curved inlet for the conditions the calibrations were performed under. The leak in the calibration assembly produced a problem in this calculation. While on the ground, the leak in the calibration assembly had little effect. Typically winds were light and the assembly had been left purging with N₂ for several hours before diode mappings were performed. Under these conditions the housing appeared to be fully flushed with N₂. However once airborne, exposure to winds of >100 m s⁻¹, and pressure changes associated with changing altitude, allowed the interior to fill with ambient air, resulting in additional attenuation of 184.9 nm light exiting the assembly due to absorption from O₂ and H₂O within the lamp assembly itself. If not accounted for, this attenuation causes an overestimate of the calculated amount of OH produced by the calibration assembly, which results in a calibration coefficient which overestimates ambient OH.

It should be possible to correct for the effects of this leak using the same approach as used in calculating the photon flux from the lamp. If the flux exiting the lamp assembly, calculated from the ground based diode mappings with the assembly fully purged with N₂, is assumed to be the flux produced by the lamp, this value can then be corrected to account for the additional absorption, caused by the leak, occurring over the path length within the lamp assembly. One drawback to this approach is that the absorption cross-section for O₂ is dependent upon both the lamp characteristics and O₂ column concentration [Creasy *et al.*, 2000]. As pointed out by these authors, to accurately use this technique, it is necessary to measure the O₂ absorption cross-section at the various O₂

column concentrations the calibrations were performed under. Thus, laboratory tests were performed where the O₂ absorption cross-section was measured. A mechanical determination of the path length within the lamp assembly yielded a value of 7.31 cm. An apparatus was constructed such that the O₂ absorption cross-section could be determined over a 7.26 or 14.57 (7.26 + 7.31) cm path length. An identical Hg Pen Ray lamp and power supply to that used in the calibration assembly were employed (mounting considerations prevented the use of the actual lamp and power supply). Light intensity at 184.9 nm was measured using a solar blind photo diode. The entire lamp/absorption cell/detector assembly was placed in an N₂ flushed housing. O₂ column concentrations were varied in the 2 - 85 x 10¹⁸ molecule cm² range. Tests performed either with or without a 184.9 band pass filter yielded identical results. O₂ column concentrations of 20 and 75 x 10¹⁸ molecule cm² (the same column concentration range as field determinations, either in situ calibrations or diode mappings, were performed under) yielded cross-sections of 12.3 and 8.6 x 10²¹ cm² molecule respectively. The measured cross-section for an O₂ column of 5.5 x 10¹⁸ molecule cm² is 1.48 x 10⁻²⁰ cm² molecule, a value in reasonable agreement with the results of *Creasy et al.* [2000], *Hofzumahaus et al.* [1997] and *Lanzendorf et al.* [1997] who obtained values between 1.1 and 1.4 x 10⁻²⁰ cm² molecule.

With the O₂ column measurements in hand, the correct calibration coefficients could be calculated. Figure 2 is a plot of the calibration coefficients determined from this study versus ambient pressure. The points shown are the average values for each calibration performed, with error bars showing the calculated standard deviation (2 sigma). There are two fits shown on the plot. The solid line is the fit to the calibration values obtained in this study. This fit yielded values ~25-30% larger than those obtained in previous studies. The calibration factor is not a highly variable quantity, depending upon the ion source geometry, ion reaction time, and detection sensitivity. This

same OH, H₂SO₄, and MSA instrument configuration was also flown aboard the P3-B during the GTE Pacific Exploratory Mission – Tropics B (PEM Tropics B) study. Operationally, differences in lens voltages (which affect ion reaction times) as a function of altitude prevent comparison at all altitudes, however at sea level, identical lens voltages (ion reaction times) were used. At this altitude, calibration values of 12.46 and 10.19 molecule cm⁻³ are obtained from the fits used for TRACE-P and PEM Tropics B respectively. A sea level value of ~10 molecule cm⁻³ was also obtained from similar but not identical instrument configurations during the NSF Aerosol Characterization Experiment – 1 (ACE-1) and GTE Pacific Exploratory Mission – Tropics A (PEM Tropics A) studies. As this value is not expected to change, the ~22% difference from historical values observed here is probably attributable to the correction for the leak in the calibration calculation. One possible cause is the assumption that the assembly was filled with air at ambient conditions. The composition of the air within the assembly, particularly H₂O, is probably different than ambient due to changes in ambient pressure (altitude). Additionally, there was also probably a build up of ozone within the assembly. If the ozone concentrations reached sufficient levels, it could cause additional attenuation of the lamp output.

With the knowledge that the calibrations in the present study had additional corrections made to them, combined with the historical consistency of the calibration coefficient, the decision was made to reduce the fit for the present calibration values by 11%, such that the new sea level value is the average of the values from the present study and PEM Tropics B. This corrected fit is shown as the dashed line in Figure 2. OH, H₂SO₄, and MSA values reported for this study were calculated using this lowered “average” fit.

It should also be pointed out that there was a larger than normal spread in the comparisons of the measurement diodes with the NIST standard diode. This spread of ~±12% is about a factor of

three larger than previously observed, and is thought to be attributed to changes in the operation of the measurement apparatus. The total reported error limits are typically $\pm 60\%$ (2 sigma), with exceptions due to instrumental problems. The error value includes the $\pm 40\%$ calculated from a propagation of errors calculation which includes both the total systematic and random errors for a given measurement, and an additional $\pm 20\%$ to reflect the spread of the NIST comparisons and the use of the corrected fit. Further, the 11% change to the fit falls well within the original $\pm 40\%$ error limits.

3. Results and Discussion

a. OH Measurements and Model Comparison

The results of OH, H₂SO₄, and MSA measurements performed aboard the P-3B during TRACE-P can be found in the GTE data archive at http://www-gte.larc.nasa.gov/trace/TP_dat.htm. Data are presented as 30 s measurements using the same data acquisition technique as described in *Mauldin et al.* [2001]. As in previous airborne studies, most of the large scale variability in the data is due to changes in altitude. Smaller scale features which are observed during constant altitude legs are due to changes in [H₂O], $j(\text{O}_3 \rightarrow \text{O}(^1\text{D}))$, and/or changes in [NO].

Photochemical box model simulations of OH data were performed using a model developed at the Georgia Institute of Technology (Ga. Tech.). A full discussion of the model used for these OH simulations together with comparisons of other radical species can be found in [*Crawford et al.*, this issue]; thus only relevant details will be discussed here. The model inputs were 1 min. averages of the species measured aboard the aircraft that affect OH concentrations (O₃, $j(\text{O}_3 \rightarrow \text{O}(^1\text{D}))$, NO, CO₂, hydrocarbons, etc).

A typical comparison of measured and modeled [OH] for a single flight can be found in Figure 3. Also shown is a plot of [NO] a key species in controlling the cycling of HO₂/RO₂ into OH. A relative altitude profile has been added for reference. As can be seen, there are regions where the model agrees well with measurements and others where it does not. Most of the overall fine structure observed in the measurements is also seen in the modeled values. An interesting feature on this plot is the large spike of NO which occurs at ~02:10 UTC. When NO concentrations increase to levels up to ~150 pptv, OH concentrations are enhanced due to increased cycling of HO₂ back into OH. However at NO concentrations above ~150 pptv, the accompanying NO₂ begins to act as a sink for OH via pathways that lead to the formation of HNO₃ (and HO₂NO₂). In Figure 3 it can be seen that during the NO spike (a ship plume crossing), the observed [OH] is suppressed dropping from ~5.5 x 10⁶ to ~2.5 x 10⁶ molecule cm⁻³. While not agreeing exactly with the measurements, the model also predicts a similar large scale decrease in OH. A plot of measured versus modeled [OH] for flights 4-24 (all flights during the TRACE-P campaign) is shown in Figure 4. As can be seen with the exception of a few outlying points, the agreement is generally good. A linear regression with a zero intercept of this data yields a slope 0.89. A standard regression yields a slope of 0.85 and an intercept of 5.22 x 10⁵ molecule cm⁻³. The slope of either regression indicates that the model has a slight tendency to under-predict OH concentrations when compared to the present measurements. This type of figure is good at revealing average overall trends; however it is not good at elucidating specific types of dependencies. A cursory look at the agreement between measured and modeled values in Figure 3 reveals that the modeled values are lower than measurements at low altitudes and larger at high altitudes. Figure 5 is a plot of the ratio of measured to modeled [OH] versus altitude. As can be seen, at sea level the ratio is on average ~1.5 indicating that the model is underestimating [OH] compared to measurements. As altitude increases the

average ratio drops to unity at ~ 0.8 km and then falls to a more or less constant value of ~ 0.8 at altitudes greater than 2 km. It is this large number of measurements made above 2 km that are dominating the fewer measurements below 2 km to give an overall agreement of 0.85-0.89, depending upon the regression used.

Putting the present overall trend value of 0.85 (the slope from the same type of regression as used in these studies) into historical perspective, it compares well with the central pacific values of 0.86 and 0.80 obtained during the PEM Tropics B study by *Tan et al.* [2001a] and *Mauldin et al.* [2001] respectively. This contrasts to the generally poor agreement with the continental values of 0.7, 0.5, and 0.38 obtained by *Carslaw et al.* [1999], *Carslaw et al.* [2001] and *Tan et al.* [2001b] respectively. When compared to the values obtained in the Tropospheric Ozone Production about the Spring Equinox (TOPSE) study, the present value agrees with the value of 0.8 obtained at higher latitudes ($>70^\circ\text{N}$), but doesn't agree very well with the value of 0.6, obtained at lower latitudes ($<57^\circ\text{N}$) [*Mauldin et al.*, accepted 2002]. The altitude trend of underestimating OH at low altitudes and overestimating OH at high altitudes in the model agreement has also been observed in previous studies [*Mauldin et al.*, 1999, 2001; *Tan et al.*, 2001a], and is also present in model simulations of OH data obtained aboard the DC-8 during TRACE-P [*Crawford et al.*, this issue]. An inter-comparison of OH and other data obtained from both the P-3B and DC-8 aircraft during three close proximity flight legs can be found in *Eisele et al.*, [this issue].

As pointed out by *Mauldin et al.* [accepted 2002], *Tan et al.* [2001a,b] and *Carslaw et al.* [2001,1999 (and references therein)], the tendency for models to overestimate OH concentrations seems to be enhanced for measurements performed in continentally influenced air. One historically common explanation is the presence of one or more unaccounted for hydrocarbon compounds which act as OH sinks [*McKeen et al.*, 1997]. In continentally influenced regions, where biogenic

carbon production is larger and transport of hydrocarbons and other compounds from local sources can increase the hydrocarbon loading, models begin to overestimate OH concentrations. What is interesting in this study is that while the measurements were performed over water, they were obtained in regions of continental outflow. One possibility for the better agreement in this region of continental influence, compared to other studies, is the addition of HO₂ and HO₂ + RO₂ measurements [*Cantrell et al.*, this issue] to the model. These two radicals are key species in the HO_x cycle and the addition of their measurement is expected to improve OH simulations.

One other possibility is that the lifetime(s) of this/these hypothesized unaccounted for hydrocarbon(s) is sufficiently short that they are substantially reduced or removed during transport from the continent out over water. Assuming a 24 hour averaged OH concentration of 1×10^6 molecule cm⁻³ (a typical value for this study), and a hydrocarbon transport time (lifetime) of 0.5 – 1.5 days (reasonable for this study), rate coefficients of $2.3 \times 10^{-11} - 7.7 \times 10^{-12}$ cm³ molecule⁻¹ s⁻¹ are obtained for reaction with OH. These values range from being extremely fast to falling in between the rate coefficients for OH reacting with propane and ethane.

b. H₂SO₄ Measurements in Volcanic Plume

The dynamic range of the instrument can be seen in the H₂SO₄ values from P-3B flight 17. The lower panel in Figure 7 is a plot of the observed H₂SO₄ values from this flight together with SO₂, the primary source of H₂SO₄ in the troposphere. Also shown in the lower panel is a relative altitude profile for reference. This flight was flown to the south-east off the southern coast of Japan. During the flight, a volcanic plume from Miyaka, Japan was encountered in the boundary layer, characterized by large concentrations (>10 ppbv) of SO₂ and an absence of CO. As can be seen, the concentrations of H₂SO₄ during these periods are also extremely large with values greater than 10^8 molecule cm⁻³. At these temperatures and humidities, these high concentrations of H₂SO₄ are

usually accompanied by high concentrations of 3-4 and 3-8 nm particles indicating new particle formation [Weber *et al.*, 1995, 1999]. Shown in the upper panel of Figure 7 is a plot of total (3 to ~200 nm) Ultra-fine Condensation Nuclei (UCN), 3-8 nm UCN, and 3-4 nm UCN. The total UCN values have been divided by 100 so that they would scale with the other UCN values. As can be seen, the total UCN is quite high with values greater than 8000 cm^{-3} during the plume encounters. During the extreme H_2SO_4 spikes, the values of 3-4 nm and 3-8 nm UCN are also seen to rise, indicating the nucleation of new particles.

c. Nighttime Flight Off Midway Island

An example of the precision the instrument is capable of when measuring low OH is P-3B flight 21, flown in the dark out of Midway Island. These types of flights are also good checks for possible interferences as OH concentrations are typically $< 10^5 \text{ molecule cm}^{-3}$ during the night for remote environments. Figure 7a is a plot of the observed [OH] during this flight. Shown are the individual 30 second measurements and 5 minute averages. Also shown is an altitude profile for reference. With the exception of some noisy excursions, it can be seen the 30 s values are less than $2 \times 10^5 \text{ molecule cm}^{-3}$, a typical limit of detection for a single measurement. 5 minute averages during these periods yield values $< 5 \times 10^4 \text{ molecule cm}^{-3}$.

The noisy periods shown in Figure 7a are actually the indication of something quite unusual. The flight path was a straight line to the southwest, and a straight line return with boundary layer runs occurring at three fairly evenly spaced locations on the linear flight path. As can be seen from the altitude profile, the noisy periods occur during the portions of the flight flown in the boundary layer. Figure 7b is a plot of the H_2SO_4 and MSA concentrations from this same flight. As can be seen, both H_2SO_4 and MSA show a marked increase during these time periods, with H_2SO_4 reaching levels of $4\text{-}6 \times 10^6 \text{ molecule cm}^{-3}$, and MSA in excess of $10^7 \text{ molecule cm}^{-3}$. The fact that such large

concentrations of these two relatively short lived, photo-chemically produced species are observed during the night is quite remarkable. Takeoff for this flight was ~1 hr after local sunset. Typical lifetimes for H₂SO₄ and MSA in a clean environment are ~20 min. The concentration levels of H₂SO₄ are on par with those seen during the day on the flights off Asia. Gas phase MSA concentrations such as these are typically only seen in much higher, dryer environments [Mauldin *et al.*, 1999].

These observations raise the concern that the large values could be due evaporation of H₂SO₄ and MSA from the inlet surfaces. Large increases in temperature or drops in relative humidity could cause an increase in the vapor pressure of H₂SO₄ or MSA absorbed on the surface of the 1.9 cm curved inlet. The effect of evaporation has been observed by our group only once before [Mauldin *et al.*, 1998], and then only at high altitude where the relative humidity fell below 5%. During the descents to these boundary layer runs, the temperature only changed by ~30 °C going from approximately -10 to +20 °C. The relative humidity during these boundary layer runs never fell below 80%. From the work of Marti *et al.* [1998], increasing the relative humidity from 5 to 80% decreases the vapor pressure of H₂SO₄ some 4 orders of magnitude. Field observations of MSA indicate that it has a similar but weaker response to relative humidity [Mauldin *et al.*, 1998]. Thus, previous flight experience with the inlet and laboratory measurements of H₂SO₄ vapor pressure both would indicate that evaporation of H₂SO₄ and MSA is insignificant for the conditions of the boundary layer portions (or the rest of) of this flight.

In order to maintain these daytime like concentrations of these two relatively short lived species, production of H₂SO₄ and MSA must be occurring. In the marine environment, these two compounds are primarily produced via oxidation of reduced sulfur, emitted from the oceans primarily in the form of dimethyl sulfide, DMS, [Bates and Cline, 1985; Andreae *et al.*, 1985].

Once in the atmosphere, DMS is oxidized by OH via a branched mechanism to produce either SO₂, much of which eventually forms H₂SO₄, or products which can lead to the formation of MSA, [Ayers *et al.*, 1991; Yin *et al.*, 1990; Toon *et al.*, 1987; Hataleyama *et al.*, 1982]. Figure 7c is a plot of SO₂ and DMS concentrations also measured during this flight. As can be seen, both species exhibit concentration peaks during the boundary layer portions of the flight. The DMS concentrations are not large with boundary layer values increasing over time from ~5 pptv to ~25 pptv. The SO₂ concentrations are also modest with values of ~50 pptv during all three boundary layer legs. The concentrations of both SO₂ and DMS, while small, do indicate the presence of two known reactants that, when oxidized via OH, produce H₂SO₄ and MSA respectively. However the key oxidizer, OH, is not present; and this oxidation is occurring at night.

An interesting exercise is to perform a crude “equivalent OH” behavior calculation for this “mystery” nighttime oxidizer. If a daytime scenario is assumed with production of H₂SO₄ from SO₂ being in steady state equilibrium with its loss, an “equivalent OH” concentration can be obtained from the SO₂ and H₂SO₄ measurements, assuming H₂SO₄ is formed from OH + SO₂. Once formed, gas phase H₂SO₄ has an atmospheric life time on the order of an hour or less, being lost by condensation, rain out, or dry deposition. To properly calculate the H₂SO₄ lifetime, the particle surface area as a function of particle size needs to be known. Unfortunately, these values are not presently available, forcing the assumption of a H₂SO₄ lifetime. Here average respective SO₂ and H₂SO₄ concentrations of 1.23 x 10⁹ (50 pptv) and 5 x 10⁶ molecule cm⁻³ and a rate coefficient of 8.83 x 10⁻¹³ cm² molecule⁻² s⁻¹ for OH + SO₂ + M → H₂SO₄ + M [DeMore *et al.*, 1997] were employed. H₂SO₄ lifetimes of <1 hour were assumed. Equivalent OH concentrations of 1.27-15.8 x 10⁶ molecule cm⁻³ are obtained for H₂SO₄ lifetimes of 1 hour and 5 minutes, respectively, using this approach. While the equivalent OH value for a H₂SO₄ lifetime of 5 minutes (an extremely short

lifetime) is large, lifetimes of 10 minutes to 1 hour yield values in the mid 10^6 molecule cm^{-3} range, on order with daytime measurements.

Once formed in the gas phase, H_2SO_4 plays an important role in particle formation and growth. In areas away from the Earth's surface, condensation of H_2SO_4 is thought to occur predominately on the surface of pre-existing aerosol particles [Clarke *et al.*, 1996; Ayers *et al.*, 1991]. However, gas phase H_2SO_4 is thought to initiate new particle formation, if the existing particle surface area is small [Covert *et al.*, 1992; Hoppel *et al.*, 1994]. As previously mentioned, UCN was also measured during this flight. An analysis of this data during the boundary layer runs not only reveals the presence of larger more aged UCN with diameters <200 nm, but also the presence of 3-4 nm and 3-8 nm UCN, indicating recent particle nucleation – at night.

As stated above, the MSA concentrations observed during the boundary layer runs are more typical of higher dryer environments. In the remote marine environment, gas phase MSA is thought to be produced from the oxidation of DMS via OH. This oxidation can proceed via abstraction or addition channels, both of which produce MSA [Davis *et al.*, 1998, 1999]. Other products include SO_2 (which ultimately forms H_2SO_4), dimethyl-sulfoxide (DMSO), dimethyl-sulfone (DMSO_2), and methane-sulfinic acid (MSIA). The overall temperature dependence of the reaction increases the final MSA/ H_2SO_4 as the temperature decreases. Previous studies in areas with similar temperatures and much higher DMS production have yielded boundary layer daytime gas phase MSA concentrations on the order $<10^6$ molecule cm^{-3} ; levels substantially lower than those observed here in the dark [Mauldin *et al.*, 1998, 1999, 2001]. Thus, to maintain the concentration levels observed here, the production of gas phase MSA here at night must be greater than that from the OH + DMS reaction observed in those previous studies.

Here two different possibilities can be considered: a) the mechanism of DMS reacting with this nighttime oxidant is more efficient at producing MSA, than the OH + DMS reaction, or b) MSA is being produced via the oxidation of some other species. As the presence of this nighttime oxidant is only being inferred by the presence of short lived oxidation products, any comment on a reaction mechanism with DMS would be speculation. However, there may be evidence that DMS is not the primary reactant. As can be seen from Figure 7c, the boundary layer concentration of DMS appears to be increasing over the evening, rising from 5 pptv on the first boundary layer leg, to 25 pptv on the last. The first and third legs were flown in the same area about 4 hours apart. This type of profile of DMS increasing over the evening has been observed before [Davis *et al.*, 1999; Nowak *et al.*, 2001], in an area with DMS production and little or no removal. Assuming DMS is the primary source of MSA, the rate of production (flux) DMS must be larger than the rate of removal by this nighttime oxidant for the same type of profile to be observed in the present study. This is a conclusion not out of the realm of possibility, however, it must be pointed out that it is a multi-step reaction with OH that yields MSA from DMS, and presumably would be so with this nighttime oxidant.

In the OH abstraction channel with DMS, MSA is produced via the formation of a CH_3S radical followed by reactions involving O_3 , HO_2 , or NO [Davis *et al.*, 1998]. The OH addition channel produces MSA via the formation of DMSO, followed by further reaction with OH. Comparing the rate coefficients for reaction with OH, one finds the DMSO rate coefficient is more than 100 times faster than that for DMS [DeMore *et al.*, 1997; Hynes and Wine, 1986]. If the same holds factor holds true for the nighttime oxidant, it would take very little DMSO to produce the observed concentrations of MSA. The role of heterogeneous reactions could also be important in this oxidation. Jefferson *et al.* [1998] postulate that the large particulate concentrations of MSA

observed during the ground based SCATE study on the Palmer Peninsula Antarctica, were due to condensed phase oxidation of DMSO. The high solubility of DMSO and the low vapor pressure of MSA would tend to preclude these sorts of reactions as being strong gas phase sources of either compound.

Recently *Nowak et al.* [2001] have reported results from the GTE PEM-Tropics B study, indicating the possibility that DMSO may be produced at night. In that study the authors measured predawn boundary layer DMSO concentrations of 5-15 pptv. The DMSO concentration profiles were significantly out of phase with model predictions which assumed DMSO to be produced only from the OH initiated oxidation of DMS. In fact the measured diurnal DMSO profiles closely tracked the observed DMS profiles, increasing until the daylight hours and then decreasing. To reconcile differences between measurements and model predictions for the PEM-Tropics B study and to explain previous ground based DMSO observations, the authors point to an alternative DMSO source, possibly the ocean itself. The high solubility of DMSO in H₂O, makes it difficult to understand how the ocean can be a very large source of gas phase DMSO, except possibly during large sea spray events. In light of the present results, another possible explanation of the observations of *Nowak et al.* [2001] could be the formation of DMSO by the nighttime oxidation of DMS. There is some evidence of this possibility seen in the H₂SO₄ and MSA data obtained during the same PEM-Tropics B flight focused on by *Nowak et al.* [2001]. That flight was flown in the early morning such that the first boundary layer leg occurred around local sunrise. While not obtained in the dark, the H₂SO₄ and MSA concentrations were quite high for that time of day, with averages of $\sim 5 \times 10^6$ and $\sim 8 \times 10^6$ molecules cm⁻³ respectively [*Mauldin et al.*, 2001]. Unfortunately, DMSO was not measured during the present study, thus its role in this nighttime oxidation chemistry remains speculative.

4. Summary and Conclusions

Combined with other parameters measured aboard the P-3B, the OH data set presented here allows an extensive comparison with model simulations over a broad range of ambient conditions. The overall average model agreement value of 0.85 is very similar to the values of 0.80 and 0.86 observed during the PEM Tropics B study [Tan *et al.*, 2001a; Mauldin *et al.*, 2001]. As the bulk of the measurements were performed in areas of Asian outflow, it is surprising that the agreement is quite better than the continental values of 0.7, 0.5, and 0.38 obtained by Carslaw *et al.* [1999], Carslaw *et al.* [2001] and Tan *et al.* [2001b] respectively.

Similarly the H₂SO₄ values provided allow a somewhat complete analysis of sulfur oxidation chemistry going from the initial reactant of SO₂ to the final product of UCN particles. The levels of H₂SO₄ encountered in the boundary layer during the volcanic plume, represent some of the largest values observed in the marine boundary layer.

The observation of high levels of H₂SO₄ and MSA, during the night is quite interesting. As these are two short lived species, the concentrations observed indicate that significant production of these species is occurring. Measurable quantities of SO₂ and DMS, two compounds which when oxidized produce H₂SO₄ and MSA, were observed; however, OH concentrations during these periods were essentially zero. The finding of evidence of nighttime oxidation in the remote marine boundary layer is unique. From the results presented, it would appear that this, yet to be determined, oxidant has a reactivity on the order of that of OH.

Evidence of nighttime oxidation has been seen before [Cantrell *et al.*, 1997; Hu and Steadman, 1995, Berresheim, private communication]. Cantrell *et al.*, [1997] saw evidence of nighttime peroxy radical formation during the MLOPEX 2c study. In that study, the authors

postulated NO₃ radical chemistry as a possible explanation for their results. As these measurements were performed in the remote marine boundary layer, NO_x/NO_y levels were low. Measurements aboard the P-3B revealed average values of 0, 5, and 200 pptv for NO, NO₂, and NO_y respectively during the boundary layer segments, indicating little possibility for NO₃ formation. Additionally, rate coefficients show that NO₃ will not significantly react with SO₂ [DeMore *et al.*, 1997]. Cantrell *et al.*, [1997] also suggested O₃ chemistry as another possible source of OH and ultimately peroxy radicals. This chemistry involves the reaction of O₃ with alkenes to forming a Criegee radical and ultimately OH. It is doubtful that this chemistry can explain the results of the present study. The OH measurements during the boundary layer portions are scattered about zero and never rise above 2.2 x 10⁵ molecule cm⁻³, a value far too low to maintain such high concentrations of H₂SO₄ and MSA. Additionally, as in Cantrell *et al.*, [1997], the measured concentrations of O₃ and alkenes during the boundary layer segments are too low to maintain the levels of H₂SO₄ and MSA observed. The large concentrations of MSA observed in themselves present a question regarding a possible mechanism. Known DMS oxidation chemistry involving OH cannot account for the MSA to H₂SO₄ ratios observed. While not measured, the high reactivity, and easier avenue to MSA, makes DMSO a more likely candidate as the direct source. Recent work by Nowak *et al.*, [2001] has demonstrated the likelihood that DMSO is produced at night, possibly by the ocean itself. As pointed out by these authors, the high solubility of DMSO makes it difficult to see how that mechanism could explain the observed gas phase DMSO values. A possible mechanism which could explain the results of Nowak *et al.* [2001] and those of the present study would be the formation of DMSO from the nighttime oxidation of DMS. This DMSO could be further oxidized to form MSA. To explain the observed boundary layer MSA/H₂SO₄ ratios, this oxidant must be more efficient at producing

DMSO (and ultimately MSA) from DMS than is OH. These observations only add to the already complicated puzzle of marine boundary layer chemistry.

5. References

Andreae, M.O., R.J. Ferek, F. Bermond, K.P. Byrd, R.T. Engstrom, S. Hardin, P.D. Houmère, F. LeMarrec, and H. Raemdonck, Dimethyl sulfide in the marine atmosphere, *J. Geophys. Res.*, *90*, 12891-12900, 1985.

Ayers, G.P., J.P. Ivey, and R.W. Gillett, Coherence between seasonal cycles of dimethyl sulfide, methane sulfonate, and sulfate in marine air, *Nature*, *349*, 404-406, 1991.

Bates, T.S., and J.D. Cline, The role of the ocean in a regional sulfur cycle, *J. Geophys. Res.*, *90*, 9168-9172, 1985.

Cantrell, C.A., G. Tyndall, and A. Zimmer, Absorption cross-section for water vapor from 183 to 193 nm, *J. Geophys. Res.*, *24*, 2195-2198, 1997.

Cantrell, C.A., G. D. Edwards, S. Stephens, R. L. Mauldin, M. Zondlo, E. Kosciuch, F. L. Eisele, R. E. Shetter, B. L. Lefer, S. Hall, F. Flocke, A. Weinheimer, A. Fried, E. Apel, Y. Kondo, D. R. Blake, N. Blake, I. Simpson, A. Bandy, D. Thornton, B. Heikes, H. Singh, W. Brune, H. Harder, M. Martinez-Harder, M. A. Avery, S. Vay, J. D. Barrick, G. W. Sachse, J. R. Olsen, J. H. Crawford, Peroxy radical behavior during TRACE-P as measured aboard the NASA P-3 aircraft, this issue.

Carshaw, N., D.J. Creasey, D.E. Heard, A.C. Lewis, J.B. McQuaid, and M.J. Pilling, Modeling OH, HO₂, and RO₂ radicals in the marine boundary layer. 1. Model construction and comparison with field measurements, *J. Geophys. Res.*, *104*, 30241-30255, 1999

- Carslaw, N., D.J. Creasey, D. Harrison, D.E. Heard, M.C. Hunter, P.J. Jacobs, M.E. Jenkin, J.D. Lee, A.C. Lewis, M.J. Pilling, S.M. Saunders, and P.W. Seakins, OH and HO₂ radical chemistry in a forested region of north-western Greece, *Atmos. Environ.*, *35*, 4725-4737, 2001.
- Clarke, A.D., Z. Li, and M. Litchy, Aerosol dynamics in the equatorial Pacific marine boundary layer: microphysics, diurnal cycles, and entrainment, *Geophys Res. Lett.*, *23*, 733-736, 1996.
- Covert, D.S., V.N. Kapustin, P.K. Quinn, and T.S. Bates, New particle formation in the marine boundary layer, *J. Geophys. Res.*, *97*, 20581-20589, 1992.
- Crawford J, J. Olson, D. Davis, G. Chen, J. Barrick, R. Shetter, B. Lefer, C. Jordan, B. Anderson, A. Clarke, G. Sachse, D. Blake, H. Singh, S. Sandolm, D. Tan, Y. Kondo, M. Avery, F. Flocke, F. Eisele, L. Mauldin, M. Zondlo, W. Brune, H. Harder, M. Martinez, R. Talbot, A. Bandy, D. Thornton, and S. Vay, Clouds and trace gas distributions during TRACE-P, *J. Geophys. Res.*, (this issue).
- Creasy, D.J., D.E. Heard, and J.D. Lee, Absorption cross-section measurements of water vapour and oxygen at 185 nm. Implications for the calibration of field instruments to measure OH, HO₂, and RO₂ radicals, *Geophys. Res. Lett.*, *27*, 1651-1654, 2000.
- Davis, D., G. Chen, P. Kasibhatla, A. Jefferson, D. Tanner, F. Eisele, D. Lenschow, W. Neff, and H. Berresheim, DMS oxidation in the Antarctic marine boundary layer: Comparison of model simulations and field observations of DMS, DMSO, DMSO₂, H₂SO₄(g), MSA(g), and MSA(p), *J. Geophys. Res.*, *103*, 1657-1678, 1998.
- Davis, D., G. Chen, A. Bandy, D. Thornton, F. Eisele, L. Mauldin, D. Tanner, D. Lenschow, H. Fuelberg, B. Huebert, J. Heath, A. Clarke, and D. Blake, Dimethyl sulfide oxidation in the equatorial Pacific: Comparison of model simulations with field observations for DMS, SO₂, H₂SO₄(g), MSA(g), MS, and NSS, *J. Geophys. Res.*, *104*, 5765-5784, 1999.

- DeMore, W.B., S.P. Sander, D.M. Golden, R.F. Hampson, M.J. Kurylo, C.J. Howard, A.R. Ravishankara, C.E. Kolb, and M.J. Molina, Chemical kinetics and photochemical data for use in stratospheric modeling, *in evaluation 12, JPL Publ. 97-4*, 266 pp., Jet Propul. Lab., Pasadena, Calif., 1997.
- Eisele, F.L., and D.J. Tanner, Ion-assisted tropospheric OH measurements, *J. Geophys. Res.*, *96*, 9295-9308, 1991.
- Eisele, F.L., and D.J. Tanner, Measurement of the gas phase concentration of H₂SO₄ and methane sulfonic acid and estimates of H₂SO₄ production and loss in the atmosphere, *J. Geophys. Res.*, *98*, 9001-9010, 1993.
- Hatakeyama, S., M. Okuda, and H. Akimoto, Formation of sulfur dioxide and methane sulfonic acid in the photooxidation of dimethyl sulfide in the air, *Geophys. Res. Lett.*, *9*, 583-586, 1982.
- Hofzumahaus, A., T. Brauers, U. Aschmutat, U. Brandenburger, H.-P. Dorn, M. Hausmann, M. Heßling, F. Holland, C. Plass-Dülmer, M. Sedlacek, M. Weber, and D. Ehhalt, Reply to comment by Lanzendorf *et al.* [1997], *Geophys. Res. Lett.*, *24*, 3039-3040, 1997.
- Hoppel, W.A., G.M. Frick, J.W. Fitzgerald, and R.E. Larson, Marine boundary layer measurements of new particle formation and the effects nonprecipitating clouds have on aerosol size distributions, *J. Geophys. Res.*, *99*, 14443-14459, 1994.
- Hu, J. and D.H. Steadman, Atmospheric RO_x radicals at an urban site: comparison to a simple theoretical model, *Environ. Sci. Technol.*, *29*, 1655-1659, 1995.
- Hynes, A.J., P.H. Wine, and D.H. Semmes, Kinetics and mechanism of OH reactions with organic sulfides, *J. Phys. Chem.*, *90*, 4148-4156, 1986.

- Jefferson, A., D.J. Tanner, F.L. Eisele, D.D. Davis, G. Chen, J. Crawford, J.W. Huey, A.L. Torres, and H. Berresheim, OH photochemistry and methane sulfonic acid formation in the coastal Antarctic boundary layer, *J. Geophys. Res.*, in press 1997.
- Lanzendorf, E.J., T.F. Hanisco, N.M. Donohue, and P.O. Wennberg, Comment on: "The measurement of tropospheric OH radicals by laser-induced fluorescence spectroscopy during the POPCORN field campaign" by Hofzumahaus *et al.* and "Intercomparison of tropospheric OH radical measurements by multiple folded long-path laser absorption and laser induced fluorescence" by Brauers *et al.*, *Geophys. Res. Lett.*, 24, 3037-3038, 1997.
- Marti, J.J., A. Jefferson, X.P. Cai, C. Richert, P.H. McMurry, and F. Eisele, H₂SO₄ vapor pressure of sulfuric acid and ammonium sulfate solutions, *J. Geophys. Res.*, 102, 3725-3735, 1997.
- Mauldin, R.L. III, D.J. Tanner, G.J. Frost, G. Chen, A.S.H. Prevot, D.D. Davis, and F.L. Eisele, OH measurements during ACE-1: observations and model comparisons, *J. Geophys. Res.*, 103, 16713-16729, 1998.
- Mauldin, R.L. III, D.J. Tanner, G.J. Frost, G. Chen, A.S.H. Prevot, D.D. Davis, and F.L. Eisele, OH measurements during PEM-Tropics A, *J. Geophys. Res.*, 104, 5817-5827, 1999.
- Mauldin, R.L. III, F.L. Eisele, C.A. Cantrell, E. Kosciuch, B.A. Ridley, B. Lefer, D.J. Tanner, J.B. Nowak, G. Chen, L. Wang, and D. Davis, Measurements of OH aboard the NASA P-3 during PEM-Tropics B, *J. Geophys. Res.*, 106, 32,657-32,666, 2001.
- Mauldin, R.L. III, C.A. Cantrell, M.A. Zondlo, E. Kosciuch, B.A. Ridley, R. Weber, and F.E. Eisele, Measurements of OH, H₂SO₄, and MSA during TOPSE, submitted *J. Geophys. Res.*, 2002.
- McKeen, S.A., *et al.*, Photochemical modeling of hydroxyl and its relationship to other species during the tropospheric OH photochemistry experiment, *J. Geophys. Res.*, 102, 6467-6493, 1997.

- Nowak, J.B., D.D. Davis, G. Chen, F.L. Eisele, R.L. Mauldin III, D.J. Tanner, C. Cantrell, E. Kosciuch, A. Bandy, D. Thornton, and A. Clarke, Airborne observations of DMSO, DMS, and OH at marine tropical latitudes, *Geophys. Res. Lett.*, *28*, 2201-2204, 2001.
- Tan, D., I. Faloon, J.B. Simpas, W. Brune, J. Olson, J. Crawford, M. Avery, G. Saches, S. Vay, S. Sandholm, H.-W. Guan, T. Vaughn, J. Mastromarino, B. Heikes, J. Snow, J. Podolske, and H. Singh, OH and HO₂ in the tropical Pacific: Result from PEM-Tropics B, *J. Geophys. Res.*, *106*, 32667-32681, 2001a.
- Tan, D., I. Faloon, J.B. Simpas, W. Brune, P.B. Shepson, T.L. Couch, A.L. Sumner, M.A. Carroll, T. Thornberry, E. Apel, D. Riemer, and W. Stockwell, HO_x budgets in a deciduous forest: Results from the PROPHET summer 1998 campaign, *J. Geophys. Res.*, *106*, 24407-24427, 2001b.
- Tanner, D.J., A. Jefferson, and F.L. Eisele, Selected ion chemical ionization mass spectrometric measurement of OH, *J. Geophys. Res.*, *102*, 6415-6425, 1997.
- Toon, O.B., J.F. Kasting, R.P. Turco, and M.S. Liu, The sulfur cycle in the marine atmosphere, *J. Geophys. Res.*, *92*, 943-963, 1987.
- Weber, R.J., J.J. Marti, P.H. McMurry, F.L. Eisele, D.J. Tanner, and A. Jefferson, Measurements of expected nucleation precursor species and 3 to 500 nm diameter particles at Mauna Loa Observatory, Hawaii, *J. Geophys. Res.*, *101*, 14,767-14,775, 1995.
- Weber, R.J., P.H. McMurry, R.L. Mauldin III, D.J. Tanner, F.L. Eisele, A.D. Clarke, and V.N. Kapustin, New particle formation in the remote troposphere: A comparison of observations at various sites, *Geophys. Res. Lett.*, *26*, 307-310, 1999.
- Weber R.J., S. Lee, G. Chen, B. Wang, V. Kapustin, K. Moore, A. D. Clarke, L. Mauldin, E. Kosciuch, C. Cantrell, F. Eisele, D. C. Thornton, A. R. Bandy, G. W. Sachse, H. E. Fuelberg,

New Particle Formation in Anthropogenic Plumes Advecting from Asia Observed During TRACE-P, *J. Geophys. Res.* (this issue)

Yin, F., D. Grosjean, R.C. Flagan, and J.H. Seinfeld, Photooxidation of DMS and DMDS, II, mechanism evaluation, *J. Atmos. Chem.*, *11*, 365-399, 1990.

Figure Captions

1. Schematic diagram of the SICIMS instrument used for the measurement of OH, H₂SO₄, and MSA during TRACE-P. The inset shows the calibration source used for the in situ generation of OH.
2. Plot of the calibration coefficient versus altitude for calibrations obtained during the TRACE-P study. These values have been corrected for the calibration assembly leak (see text). Also shown is the fit to these values together with a fit which has been reduced by ~9%, to obtain a sea level value which is the average of the sea level values obtained in this study and PEM-Tropics B (see text).
3. Plot of measured and modeled OH concentrations for a typical flight together with observed [NO], a key specie in controlling OH. A relative altitude profile is provided for reference. As can be seen much of the high frequency changes are due to changes in [NO]. The large spikes in NO (due to a ship plume) are large enough to suppress OH by acting as a sink to HO_x (see text).
4. Comparison of measured OH values from the entire TRACE-P study together with those obtained from model simulations. A linear fit to this data yields a slope of 0.85, indicating an overall tendency for the model to overestimate measurements.
5. Plot of the ratio of measured to modeled OH versus altitude. As can be seen the model tends to under-predict measured OH at altitudes less than 1.5 km. At altitudes greater than 1.5 km the model tends to overestimate OH measurements. As the bulk of the measurements were made at

altitudes greater than 1.5 km, this overestimation dominates the overall model agreement seen in Figure 4.

6. Lower panel - Plot of $[H_2SO_4]$ and $[SO_2]$ for a flight in which a boundary layer volcanic plume from Miyaka, Japan was encountered. A relative altitude profile is provided for reference. As can be seen, both the $[SO_2]$ and $[H_2SO_4]$ are quite large during the encounters with the $[H_2SO_4]$ spiking to values greater than 10^8 molecule cm^{-3} . Upper panel – Plot of total UCN, 3-8 nm UCN and 3-4 nm UCN for the same flight. The UCN values have been divided by 100 for scale purposes. The presence of the 3-4 nm and 3-8 nm spikes indicate the presence of newly formed particles.

7. Measurements from a nighttime flight off Midway Island. Take-off for this flight was ~1 hour after sunset. a.) plot of observed $[OH]$. As can be seen the values are quite small with typical 5 min. averages $<2 \times 10^4$ molecule cm^{-3} . b.) Plot of observed $[H_2SO_4]$ and $[MSA]$ for the same flight. The boundary layer concentration of these two short lived, photo-chemically produced species is quite large for nighttime conditions. As the typical lifetimes of these compounds are short (<20 min.), these concentration levels indicate production is occurring. c.) Plot of $[SO_2]$ and $[DMS]$, two reactants known to produce H_2SO_4 and MSA. The SO_2 and H_2SO_4 measurements indicate that the oxidizing specie(s) is approximately as strong as OH (see text). Combining the very large boundary layer MSA concentrations with the rising concentrations, it is hard to explain that DMS is the primary reactant to form MSA.

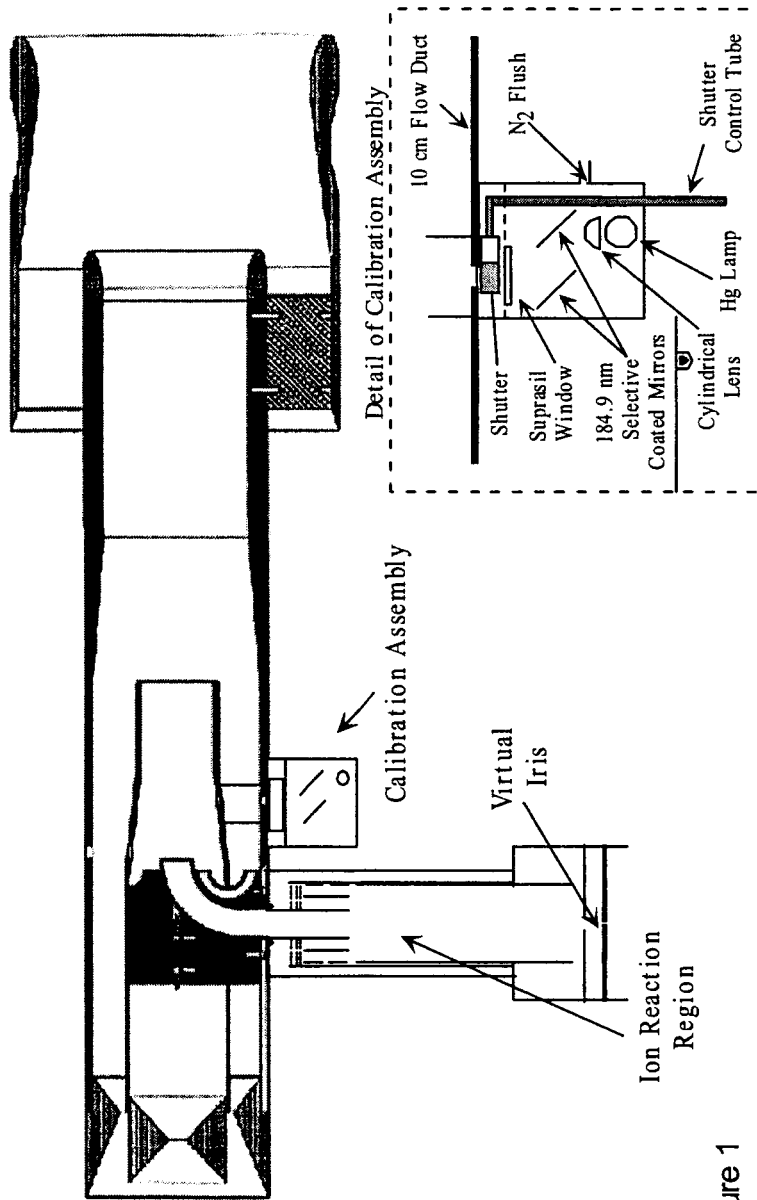


Figure 1

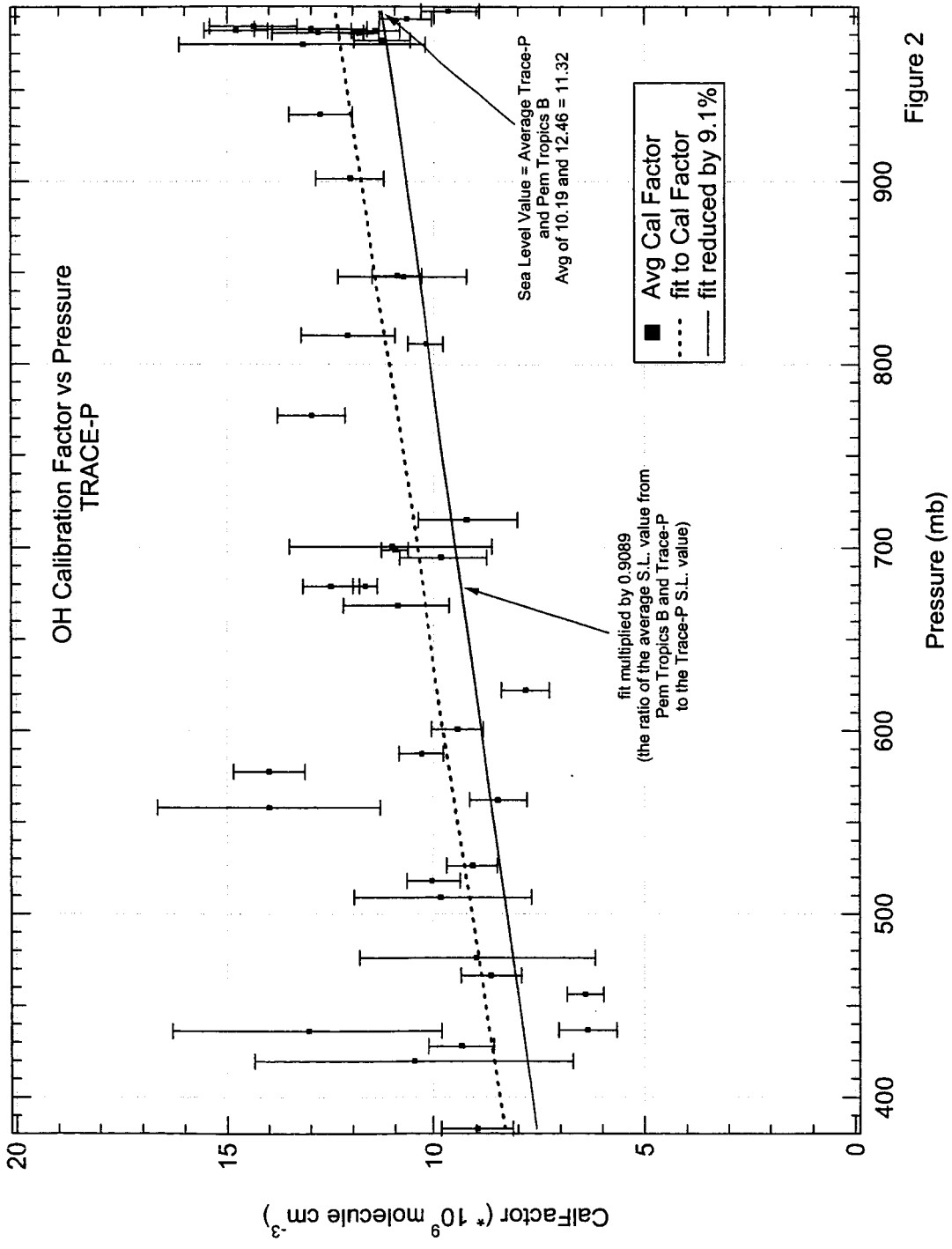


Figure 2

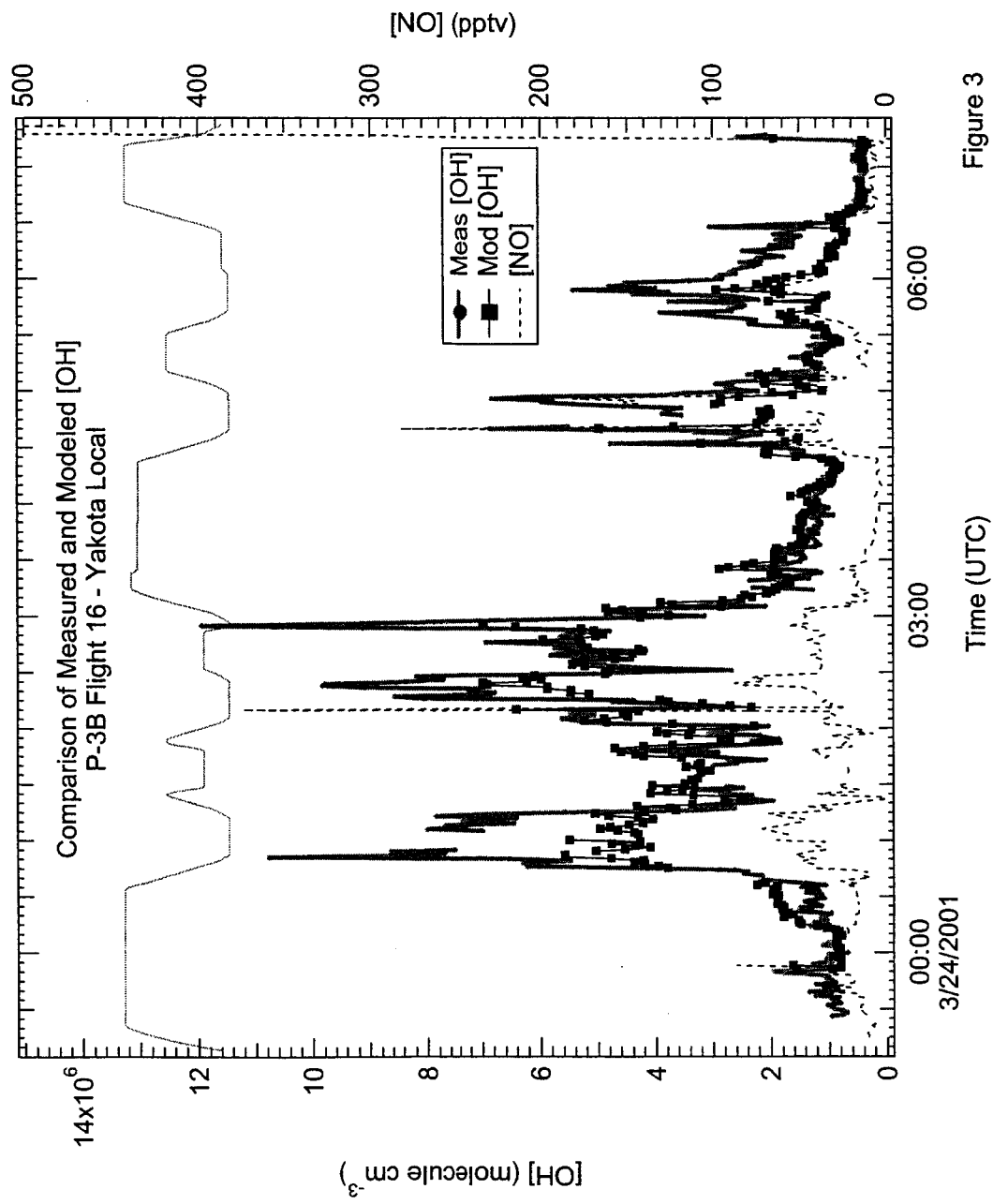


Figure 3

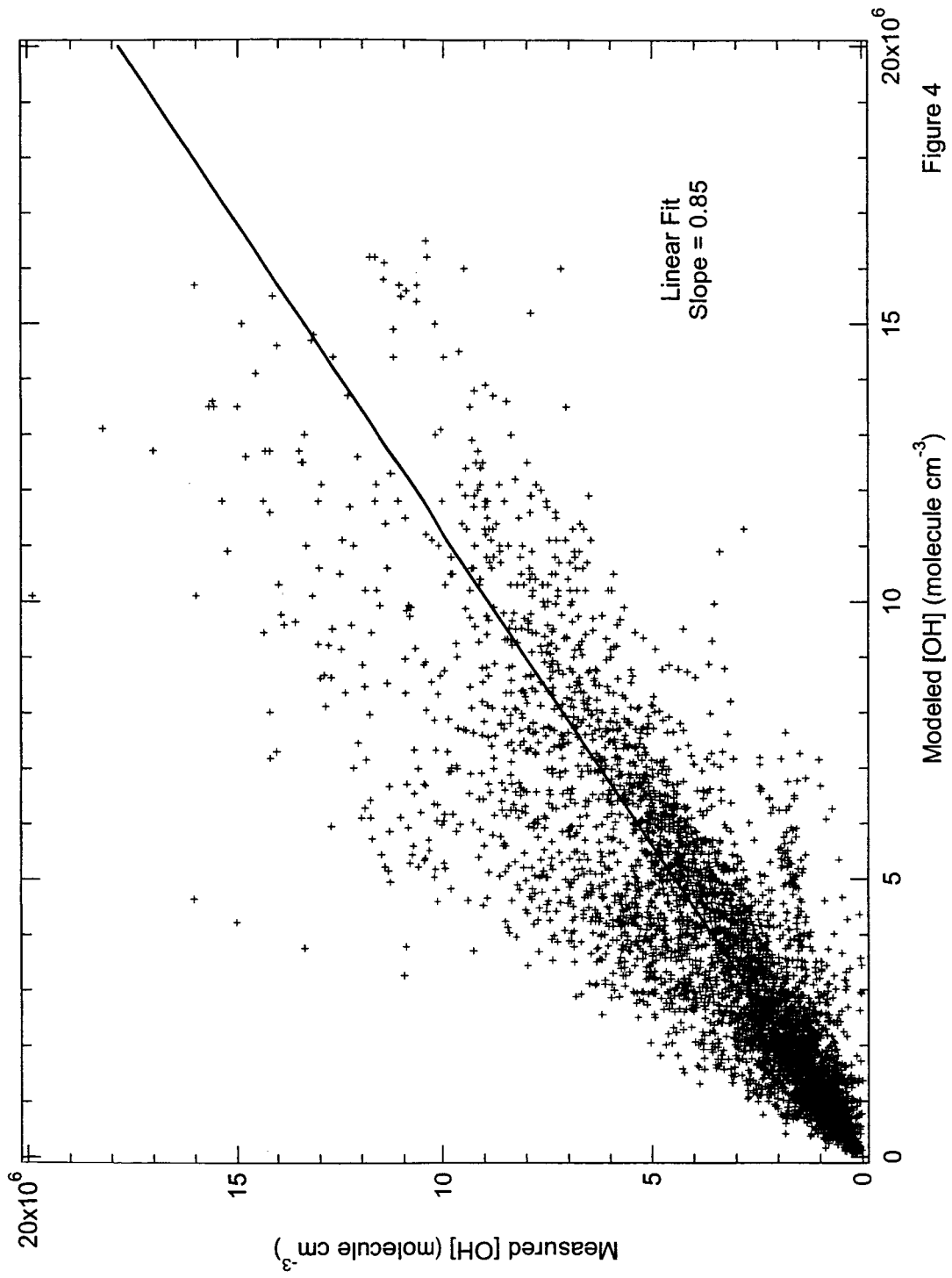


Figure 4

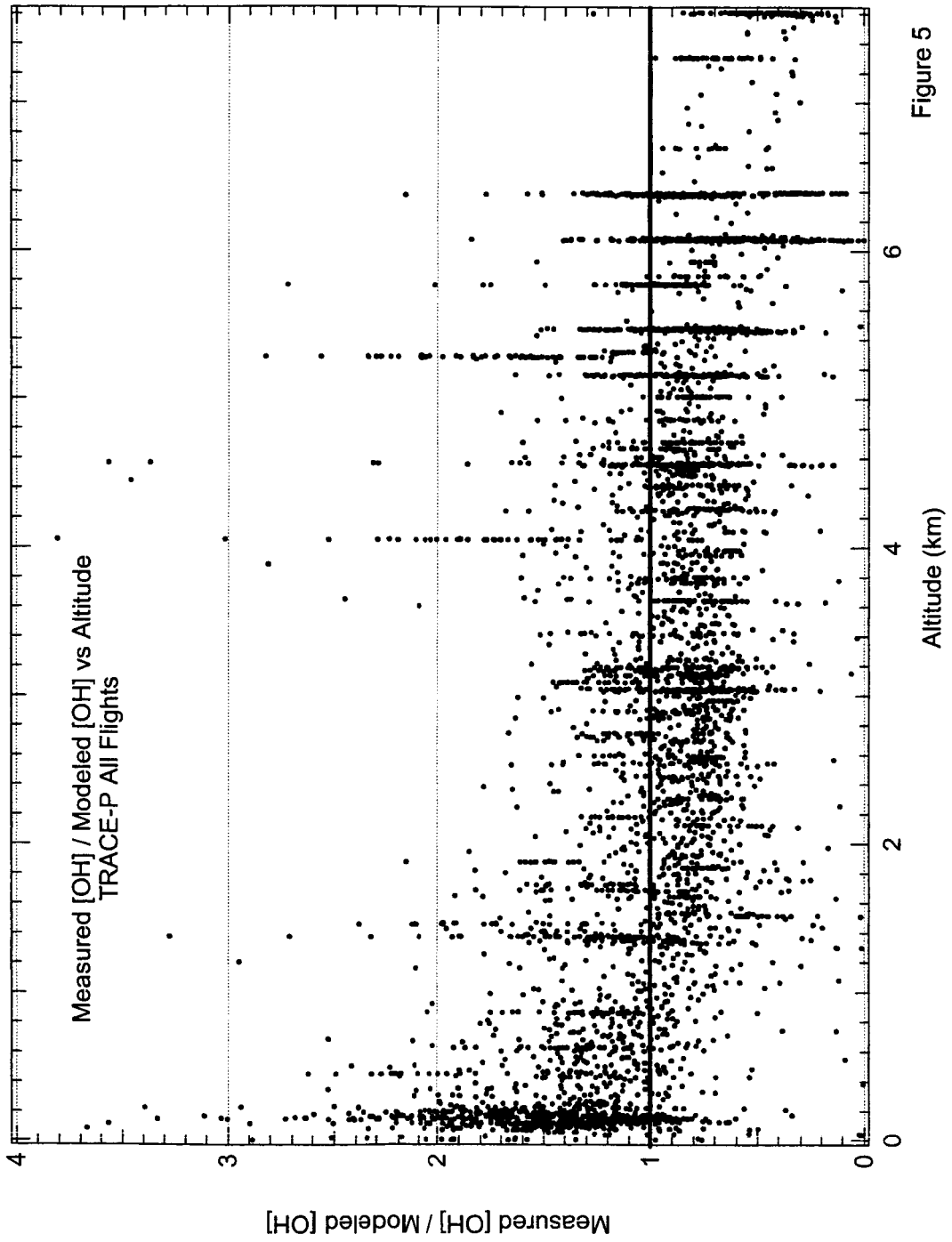
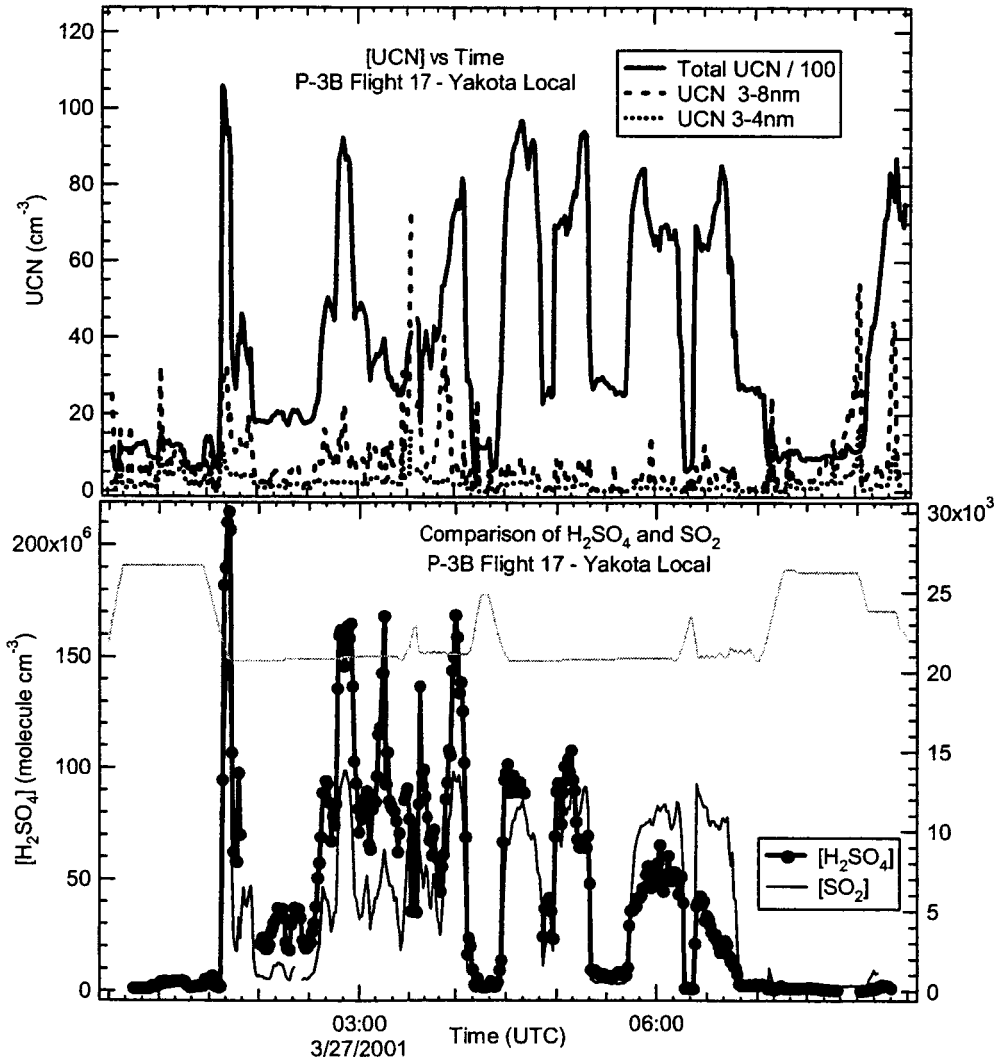


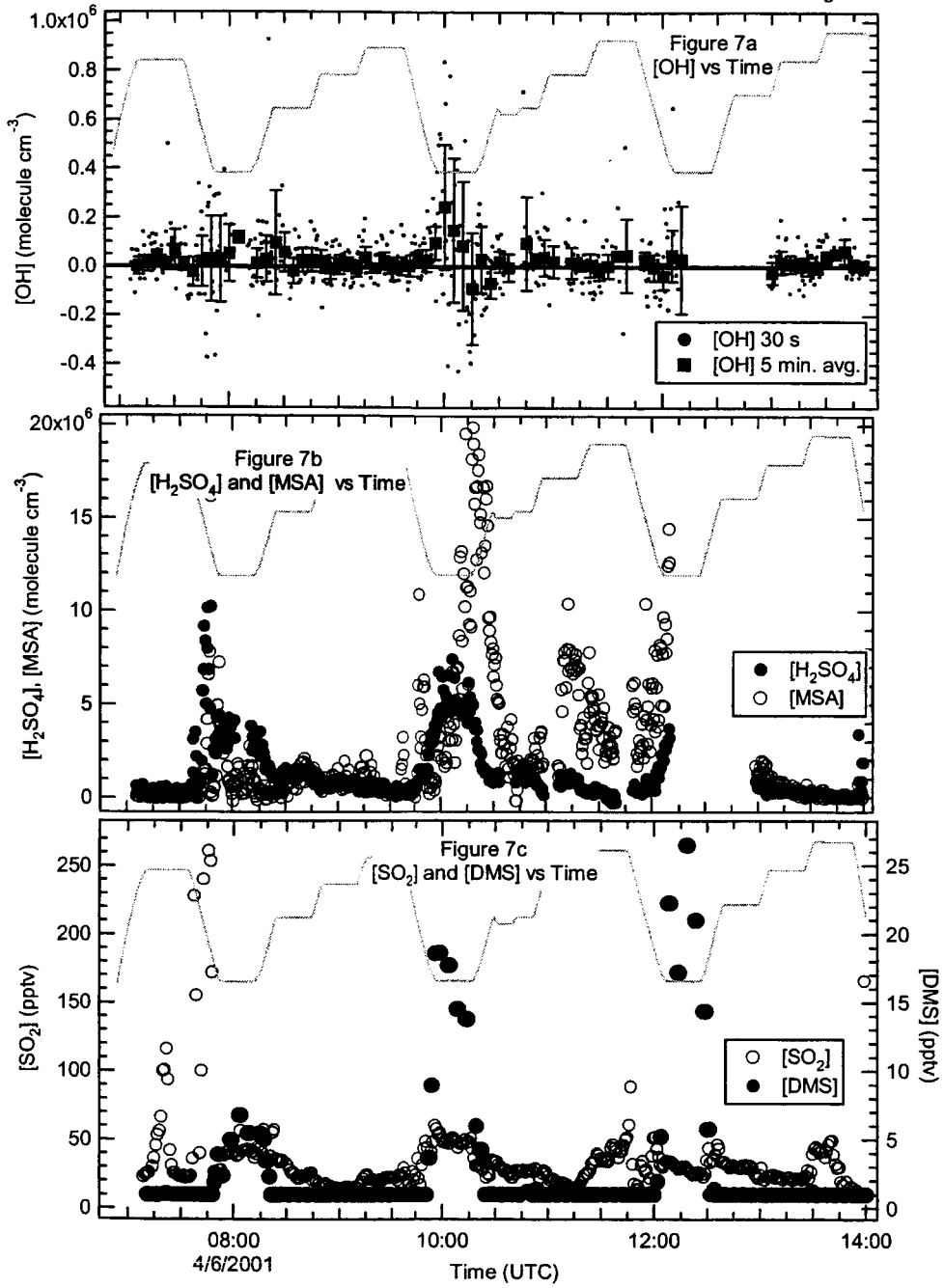
Figure 5

Figure 6



P-3B Flight 21 - Midway Local (Night Flight)

Figure 7



**Development and characterization of an airborne-based instrument used to measure
nitric acid during the NASA TRACE-P field experiment**

Mark A. Zondlo^{1,2*}, R. Leon Mauldin¹, Ed Kosciuch¹, Christopher A. Cantrell¹, and Fred L. Eisele¹

¹Atmospheric Chemistry Division and ²Advanced Study Program
1850 Table Mesa Dr.
P.O. Box 3000
National Center for Atmospheric Research
Boulder, Colorado, 80305

Submitted to *Journal of Geophysical Research – Atmospheres*
Special Section on NASA TRACE-P

Index terms

Primary: 0394 instruments and techniques

Secondary: 0365, troposphere – composition and chemistry; 0305, aerosols and particles

* To whom correspondence should be addressed:

Mark Zondlo
Southwest Sciences, Inc.
1570 Pacheco Street, Suite E-11
Santa Fe, NM 87505
Phone: (505) 984-1322
Fax: (505) 988-9230
e-mail: mzondlo@swsciences.com

Running title: Nitric acid instrument in TRACE-P

11/27/02

Abstract. A new inlet and instrument have been developed for the rapid measurement of gas phase nitric acid (HNO_3) from an airborne platform. The inlet was kept near ambient temperatures with a very short sampling time (100 ms) to minimize desorption of particle nitrates. In addition, inlet surface adsorption problems were minimized by the use of extruded perfluoro-alkoxy (PFA) as a sampling material. Nitric acid was detected by selected ion chemical ionization mass spectrometry using deprotonated methanesulfonic acid as a reagent ion. Laboratory tests showed no interferences from NO , NO_2 , NO_3 , and N_2O_5 under wet ($\text{RH}=100\%$) or dry ($\text{RH}=0\%$) conditions at levels exceeding those found in the troposphere. Nitric acid was measured every 5 s for a 3 s integration period with a limit of detection of 5 pptv. Absolute uncertainties including systematic errors are the limit of detection (5 pptv) plus $\pm 15\%$ for $\text{HNO}_3 > 200$ pptv, $\pm 20\%$ for HNO_3 100-200 pptv, and $\pm 25\%$ for $\text{HNO}_3 < 100$ pptv ($\pm 2\sigma$). The instrument was calibrated by the addition of isotopically-labeled H^{15}NO_3 near the front of the ion source on a continual basis. The inlet and instrument were flown on the NASA P-3B airplane as part of the NASA TRACE-P field campaign off the coast of Asia in February-April 2001. Rapid changes in ambient HNO_3 were resolved, suggesting minimal influences from instrument surfaces. Finally, the measurements compared favorably with the University of New Hampshire's mist chamber/ion chromatography instrument flown onboard the NASA DC-8 aircraft during two intercomparison flights. The in-flight performance of the instrument is demonstrated under the wide range of conditions observed in TRACE-P.

Introduction

Nitric acid, HNO_3 , plays important roles in both the gas phase and condensed phase chemistry of the troposphere. Gas phase HNO_3 is formed by the oxidation of the nitrogen oxides NO and NO_2 (NO_x), species that play important roles in ozone photochemistry. Tropospheric HNO_3 has a relatively long lifetime with respect to photolysis (weeks) and reaction with OH (weeks). The dominant loss mechanism is by removal onto particle surfaces, followed by either wet or dry deposition, with a heterogeneous lifetime of a few days [*Liang et al., 1998*]. In the condensed phase, HNO_3 usually dissociates into particulate nitrate, NO_3^- . The availability of gas phase HNO_3 has been shown to be important in liquid particle growth and composition [*Kerminen et al., 1997; Adams et al., 1999*]. Furthermore, HNO_3 uptake by particles indirectly affects cirrus cloud properties by altering the deliquescence behavior of salt particles [*Lin and Tabazadeh, 2002*] and by activating cloud condensation nuclei [*Laaksonen et al., 1997*]. Modeling studies suggest that gas phase HNO_3 assists in the development of unhealthy particulate matter in urban areas [*Meng et al., 1997*]. Because of the role of HNO_3 as a sink for NO_x and its significance to aerosol particle dynamics, the chemistry of HNO_3 is important towards understanding issues such as photochemical smog, acid deposition, climate change, and human health.

Numerous modeling and field studies have investigated the tropospheric chemistry of HNO_3 , and model results, though improving, can significantly differ from the measurements [*Singh et al., 1996; Jacob et al., 1996; Singh et al., 1998*]. One of the major uncertainties of HNO_3 is the partitioning between the gas and condensed phases [*Dentener et al., 1996; Adams et al., 1999*]. Based on laboratory and modeling studies, a number of atmospheric surfaces have been implicated in removing gas phase HNO_3 , but in-situ verification of these heterogeneous processes is lacking [*Dentener et al., 1996; Zondlo et al., 1997; Abbatt, 1997; Underwood et al.,*

2001]. Nonetheless, particulate nitrates are thought to be a significant component of aerosol mass, especially downwind of urban and agricultural areas [Adams *et al.*, 1999].

Understanding the chemistry of HNO₃ has been further complicated by the numerous challenges in its measurement, especially on airborne platforms where conditions change rapidly. Resolving HNO₃ concentrations in thin layers of particles, for example, requires an instrument with high sensitivity and short integration times. Furthermore, instrument surfaces should have minimal influence on the sampling of the ambient air. Otherwise, rapid changes in gas phase HNO₃ are buffered by adsorption/desorption of HNO₃ on instrument and inlet surfaces, and thus the measurements lose their time response. One method used to minimize surface effects is by heating the inlet surfaces [Neuman *et al.*, 2000; 2002]. However, heating induces the possibility that particulate nitrate may desorb into gas phase HNO₃ and thereby result in artificially inflated gas phase HNO₃ measurements. Thus, the characteristics of an ideal HNO₃ instrument for aircraft studies are high sensitivity and temporal resolution, short sampling times, inlet surfaces with minimal adsorption problems, and inlets kept as close to ambient conditions as possible.

The mist chamber/ion chromatography technique [Talbot *et al.*, 1997; Talbot *et al.*, 1999] has been used extensively on aircraft for measuring HNO₃ as well as a variety of other soluble compounds simultaneously. Briefly, ambient air is pulled into the cabin at very high flow rates (1500-3000 sLpm) and collected on a fine particle mist. The corresponding solutions are analyzed by ion chromatography. The technique is extremely reliable and sensitive (3 pptv) but has relatively long integration periods (minutes) for aircraft platforms. Furthermore, because particles less than ~ 2.5 μm in aerodynamic diameter are sampled by the inlet, fine nitrate-containing aerosols may complicate the gas phase measurements.

Airborne chemical ionization mass spectrometer (CIMS) instruments have shown high time resolution (< 1 Hz) with excellent sensitivity (> 1 count pptv⁻¹ s⁻¹) and selectivity. Neuman

et al. [2000, 2002] use SiF_5^- ion chemistry which is extremely sensitive ($1.1 \text{ ion counts pptv}^{-1} \text{ s}^{-1}$) and fast ($\leq 1 \text{ Hz}$), but their use of heated PFA inlets at 50° C may complicate the distinction between particulate and gas phase HNO_3 , particularly in polluted areas. *Arnold et al.* [1992], *Reiner et al.* [1998], *Schneider et al.* [1998] and *Miller et al.* [2000] use ion chemistry, CO_3^- (H_2O), that has the potential for interferences at the pressures of the lower and middle troposphere [*Möhler and Arnold, 1991*], and their stainless steel inlets remain well above ambient temperatures. To acquire accurate budgets of HNO_3 , unambiguous measurements of gas phase HNO_3 need to be made near ambient conditions and at high-temporal resolutions.

To this end, a new inlet and CIMS instrument design has been developed and characterized to measure HNO_3 from an airborne platform. The instrument used deprotonated methanesulfonic acid (CH_3SO_3^- , MSA) as a reagent ion for HNO_3 detection and a unique choice of inlet design and materials for the sampling of the ambient airstream. The instrument was flown on the NASA P-3B aircraft as part of the NASA Transport and Chemical Evolution over the Pacific (TRACE-P) field experiment off the coast of eastern Asia in February-April 2001. Results from the field and in the laboratory suggest that the technique has a low limit of detection (5 pptv) and a fast time response (5 s). A description of the behavior and characteristics of the instrument under a wide variety of laboratory and field conditions is presented.

Experimental

The detection of HNO_3 was conducted using selected ion chemical ionization mass spectrometry with deprotonated methanesulfonic acid (MSA) as the reagent ion. The instrument was part of a four channel mass spectrometer system also containing components to measure hydroxyl radicals (OH), gas phase sulfuric acid (H_2SO_4), and gas phase MSA [*Mauldin et al.*,

1999], and components for measuring peroxy radicals HO₂/RO₂ [Cantrell *et al.*, *this issue*]. Each channel had independent ionization schemes, flow controls, pressure controls, electrostatic lenses, quadrupoles, and electron multipliers, but they shared a common vacuum housing inside the aircraft. The vacuum housing was pumped by three 1000 L s⁻¹ turbomolecular pumps in four stages. The first stage was pumped at a pressure of 10⁻² Torr, the second stage of lenses and skimmers was pumped at 10⁻³ Torr, the quadrupoles were pumped at ~ 6 x 10⁻⁵ Torr, and the Channeltron electron multipliers in the last stage were at 3 x 10⁻⁵ Torr. The 4-channel system and corresponding inlets were located on the front, port side of the P3-B aircraft. Figure 1 shows a photo of the inlet and its location on the P3-B aircraft, and Figure 2 shows a schematic of the HNO₃ inlet and instrument. The inlet/instrument consisted of four parts: (1) a long, shrouded duct to straighten and slow the ambient airflow outside the plane, (2) a transport tube to bring the sampled air toward the airplane and for calibration, (3) an ion-molecule reaction region, and (4) the vacuum housing of ion lenses and quadrupoles inside the plane. For clarity, the general term “inlet” will refer to all parts of the instrument outside the airplane (1-3).

The shrouded duct (l=76.8 cm, 7.6 cm id, 8.9 cm od) was scaled down by a factor of 1.5 from the one described in *Eisele et al.* [1997]. The aluminum duct was tipped 9° away from the aircraft and secured at the back by an aluminum pylon that extended 15 cm from the fuselage of the aircraft (Fig. 1). The front, center of the duct was about 40 cm away from the aircraft surface, or about three times the distance that the boundary layer was calculated to expand out from the aircraft at this station. A shroud of 19.6 cm length (16.0 cm o.d., 13.3 cm i.d) had an elliptically-shaped surface to minimize turbulence effects while straightening, but not slowing, the airflow. The duct was concentric with the shroud, beginning 9.3 cm inside the shroud and continuing to the back of the pylon. The purpose of the duct was to transport the sampled air from a turbulence free region to the transport tube and to slow the flow by about an order of

magnitude relative to the free air speed (110-160 m s⁻¹) via a restricting orifice (r=1.9 cm) on the back end of the duct. Wind tunnel tests in *Eisele et al.* [1997] indicated that the airflow remained non-turbulent in the center of the duct at angles of attack less than 17°, and the scaled down version of inlet used here was expected to behave similarly.

A transport tube (2, Fig. 2), located about 65 cm downstream from the front of the duct, pulled a sample flow of 4-6 sLpm air toward the ion source region (3, Fig. 2). The transport tube (1.9 cm i.d., 2.2 cm o.d., l=10 cm), composed of extruded perfluoroalkoxy (PFA), was transverse to the duct, and its top was just below the centerline of the inner duct. The remainder of the flow in the duct (~ 10⁴ sLpm depending upon air speed and ambient pressure) was vented out the back through the restricted opening. On the forward facing side of the transport tube, a semicircle notch of r=1 cm was cut out near the top, and a PFA cap covered the top of the transport tube. In this way, the air that entered the tube generally was pulled down toward the ion source. Because the transport tube extended to the middle of the duct, it was unavoidable that turbulence developed in the duct near and downstream of the transport tube. However, air sampled by the transport tube should have had minimal contact with the aluminum surfaces of the duct up to this location. As will be demonstrated later, observational data on the response of the inlet to changes in gas phase HNO₃ concentration support this assertion.

Air sampled into the transport tube underwent an 81° deflection, and subsequent turbulence and contact with transport tube surfaces was unavoidable. Although cartridge heaters and an RTD temperature sensor were placed in the aluminum housing surrounding the transport tube, these heaters were never activated during flight and were only used to heat the inlet on-ground if necessary (e.g. for cleaning). Temperature readings indicated that the transport tube remained within 5 K of the ambient temperature during flight. Because the sampled air readily contacted the transport tube walls at near ambient temperatures and humidities, it was necessary

to find a material that was particularly inert to surface adsorption and desorption of HNO_3 . *Neuman et al.* [1999] reported that PFA tubing was an optimal choice for inlet materials for HNO_3 sampling. However, even PFA had significant adsorption problems below 10°C , and *Neuman et al.* [1999] concluded that inlets needed to be heated to at least this temperature.

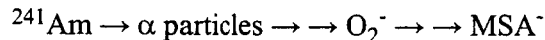
A very similar inlet to the one described above was flown on the NSF NCAR C-130 as part of the Tropospheric Ozone Production about the Spring Equinox (TOPSE) field campaign from Feb.-May 2000 from Colorado northward to the Arctic Ocean. Although no robust HNO_3 measurements were made during this campaign due to numerous problems, significant advances were made in inlet design and characterization from in-flight tests. The inlet initially used regular (machined) PFA as a choice for a sampling tube with the finding of similar conclusions by *Neuman et al.* [1998]. In other words, whenever the inlet became even slightly cold, the response of the inlet to changes in gas phase HNO_3 was very slow (timescale of minutes for a factor of ten change in concentration). To help mitigate this problem, an extruded PFA tube replaced the machined PFA tube, and it showed excellent response, even under very cold conditions. Presumably, extruded PFA has significantly less surface area and is less porous than machined PFA, thereby giving far superior transmission of gas phase HNO_3 down the tube. Finally, it is important to note that the dimensions of the transport tube used in TRACE-P (1.9 cm in diameter and only ~ 10 cm long) also helped to minimize the available surface contact with ambient air.

Based on the C-130 flights in TOPSE and additional results from the laboratory, extruded PFA was the material of choice for the transport tube on the NASA P-3B aircraft. Therefore, the turbulence and temperature of the sampled air inside the transport tube were no longer a major concern. Three additional flows were added in the transport tube. First, about 3 cm below the top of the tube, a series of holes 1 mm in diameter encircled the circumference of the tube (not

shown in Figure 2 for clarity). These holes allowed for the addition of zero air into the top of the transport tube for examining the amount of HNO_3 adsorbed onto the inlet surfaces downstream of this point. A second hole about 5 cm down from the top of the transport tube allowed for the introduction of a 1.1 mm o.d., 0.6 mm i.d. tube to flow isotopically-labeled H^{15}NO_3 for calibration. Finally, a flow of zero air could be added to the ambient air at the end of the transport tube immediately before entering the ion source. This flow was most often used to examine for background signals of HNO_3 downstream from the transport tube.

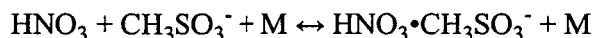
The ambient air next passed through a removeable type 316 stainless steel tube ($l=8.76$ cm, $id=1.22$ cm, $od=1.27$ cm) to enter the ion source (3, Fig. 2). This tube, although relatively short, was composed of stainless steel in order to remain at ground potential (uncharged). A notched TFE collar around the outside of the stainless steel tube kept it secured in-flight and also served as the source of the reagent ion, methanesulfonic acid (MSA, $\text{CH}_3\text{SO}_3\text{H}$). MSA was physically applied to a 0.05 cm indentation in the TFE by rubbing a piece of PFA tubing dipped in MSA (J.T. Baker, 99.7%) to ensure a visual even distribution of small droplets. MSA was applied to the TFE collar before every flight, and the entire MSA assembly (TFE collar and s.s. tube) was manually placed into the ion source. Similarly, the MSA assembly was removed and cleaned immediately after flight to prevent MSA from significantly coating the surfaces of the ion source while on the ground. Any residual MSA on other parts of the ion source were removed by heating the entire ion source and transport tube while on the ground.

A flow of ~ 3 sLpm zero air, termed "sheath flow", was distributed around the outside of the stainless steel tube through a showerhead assembly of 0.75 mm holes and fine mesh screens to minimize turbulence. The sheath flow passed over the TFE indentation and picked up MSA vapor. About 1 cm downstream of the MSA source, MSA vapor flowed over a 1.1 mCi americium-241 source and was ionized through a multistep, charge transfer process:



The radioactive source was a 0.7 cm wide strip of americium-241 radioactive in the center of a 1.3 cm x 7.2 cm gold foil. The foil was positioned 0.5 cm behind the end of the stainless steel tube and held on the outside of a 2.28 cm diameter mount. In this way, alpha particles ionized only the sheath air on the outermost, annular layer, and direct ionization (and associated radical production) of the ambient airstream was prevented.

The flow of MSA and other ions joined the flow of the ambient air at the end of the stainless steel tube. Electrostatic lenses pushed the newly created ions toward the center of the ambient stream where ion-molecule reactions occurred through a drift region of 6 cm. Initial potentials were around -350 V, and average electric fields in this region were $\sim 50 \text{ V cm}^{-1}$. The residence time of ions in the drift tube under typical flow conditions was $\sim 50 \text{ ms}$, sufficient time for the ion-molecule species to achieve equilibrium. Nitric acid clustered with MSA in the following equilibrium:



By rearranging the equilibrium equation, the concentration of nitric acid was obtained:

$$[\text{HNO}_3] = \frac{[\text{HNO}_3 \cdot \text{CH}_3\text{SO}_3^-]}{c \cdot [\text{CH}_3\text{SO}_3^-]} \quad \begin{array}{l} \leftarrow m/e \ 158 \\ \leftarrow m/e \ 95 \end{array}$$

where c is a constant calculated by adding a known amount of isotopically-labeled H^{15}NO_3 to the transport tube. In practice, the raw HNO_3 signal is the ratio of the ion counts at $m/e \ 158$ ($\text{HNO}_3 \cdot \text{CH}_3\text{SO}_3^-$) and at $m/e \ 95$ (CH_3SO_3^-). Regardless of the change of ion counts for MSA, the observed ratio will remain constant for a given concentration of HNO_3 , all other things being equal. Although the ratio will remain constant, the overall sensitivity (concentration per ion ratio) is determined by the number of MSA monomer counts.

The resulting ions were electrostatically forced downstream toward the virtual iris/pinhole plates, while the subsequent neutral species were pumped away through annular ports located downstream of the ion-molecule reaction region at a flow of ~ 9 sLpm (~ 3 Lpm of sheath, ~ 6 Lpm of ambient air). The ions were directed by electric fields through a flow of 800 sccm nitrogen in front of a virtual iris consisting of two co-aligned 0.33 mm and 0.20 mm diameter orifices on 0.25 mm thick stainless steel plates separated by 0.76 mm. The flow of dry nitrogen in front of the pinhole helped to minimize ion clustering with water. The ~ 85 Torr pressure of the interstitial space between the virtual iris plates was kept constant to ensure that a constant stream of gas entered the vacuum system at all flight altitudes and pressures [Mauldin *et al.*, 1998a].

Upon passing through the virtual iris, ions expanded supersonically into a differentially-pumped region of $\sim 10^{-2}$ Torr where a series of additional lenses applied an electric field of ~ 2 V cm^{-1} . The field strength at these relatively low pressures resulted in collisions that broke apart a fraction of weakly bound clusters into their most acidic core ions [Tanner and Eisele, 1995]. Specifically, the electric field in this region was optimized to ensure that the signals from the desired clusters of interest, $\text{MSA}\cdot\text{HNO}_3$ at m/e 158 (for ambient) and $\text{MSA}\cdot\text{H}^{15}\text{NO}_3$ m/e 159 (for calibration), were maximized, and that weaker bound species (e.g. water clusters) were broken apart. The ions were focused by three lenses into a skimmer, by four more lenses into the quadrupole mass filters, and by one back lens into a Channeltron electron multiplier. With the exception of the virtual iris, all of the inlet remained outside the fuselage of the aircraft at ambient pressures.

The choice of ion chemistry for HNO_3 detection was particularly challenging for an airborne atmospheric pressure ionization scheme. Mauldin *et al.* [1998b] previously described a ground-based CIMS technique using bisulfate (HSO_4) as a reagent ion. Unfortunately,

difficulties in maintaining a constant source of reagent ion HSO_4^- were encountered. The gas phase concentration of sulfuric acid (H_2SO_4), the reagent ion precursor species, was difficult to control due to the intrinsically very low vapor pressure of sulfuric acid and its efficient ability to cluster with itself. Therefore, HSO_4^- reagent ion chemistry was an unreliable choice for use on an airborne platform where temperatures and relative humidities change rapidly. However, HSO_4^- reagent ion chemistry did show excellent sensitivity and selectivity for detection of HNO_3 , and it was desired to keep these characteristics as much as possible. A compound of similar chemical structure and gas phase acidity was sought, but also one with significantly higher vapor pressures. To this end MSA, a derivative of sulfuric acid, was chosen. MSA is slightly more acidic ($\Delta G_{\text{acid}} = -1318 \pm 8.4 \text{ kJ mol}^{-1}$ for MSA; $\Delta G_{\text{acid}} = -1251 \pm 13 \text{ kJ mol}^{-1}$ for H_2SO_4) [Koppel *et al.*, 1994] and its vapor pressure is several orders of magnitude higher than H_2SO_4 [Ayers *et al.*, 1980; Tang and Munkelwitz, 1991]. Although MSA proved more reliable and easier to use than H_2SO_4 , as will be described in detail later, controlling the concentration of MSA in the ion source under flight conditions remained problematic at times.

Results

Laboratory. A series of laboratory experiments were performed to examine the sensitivity of the ion chemistry to potential interferences expected in the atmosphere. Specifically, the nitrogen oxide species (NO_y) NO, NO_2 , NO_3 , and N_2O_5 were tested under dry and wet conditions (relative humidity with respect to water, RH_w , 0.001-100%) at NO_y mixing ratios far exceeding those expected in the troposphere. Experiments were conducted at two different mixing ratios of H^{15}NO_3 (80 pptv and 800 pptv) to examine if the MSA/ HNO_3 and MSA/ H^{15}NO_3 ion chemistry were perturbed by the addition of these species.

NO was prepared by filling a 5 L bulb with 10 Torr of a 0.5% NO/N₂ cylinder mixture and 960 Torr of N₂. A flow of 2 sccm from the bulb was passed through approximately one meter of 3.2 mm o.d., 1.6 mm i.d. nylon tubing to help remove any residual impurities of HNO₃ in the gas source (nylon is known to be an efficient scavenger of gas phase HNO₃). The flow was then diluted into 8000 sccm of zero air over the ion source resulting in a mixing ratio of 13 ppbv NO. No change in the ratio of the H¹⁵NO₃/MSA (m/e 159) ratio was observed from the addition of the NO, nor was any increase observed for the HNO₃/MSA (m/e 158) ratio. These results indicate that NO neither produced HNO₃ in the ion source nor did it alter the HNO₃/MSA ion chemistry. Tests were done under both dry (0.001% RH) and wet (100% RH) conditions, and no noticeable change was observed in either case.

N₂O₅ was synthesized by the method of *Davidson et al.* [1978]. The N₂O₅ was stored in dry ice and kept in the dark when not in use. The N₂O₅ was differentially-pumped for several minutes prior to use at temperatures as high as 243 K. A flow of 93 sccm of N₂ was passed over the N₂O₅ which was kept in a dry ice/ethanol bath at 205 K. The vapor pressure of N₂O₅ at 205 K was approximately 6 mTorr [*McDaniel et al.*, 1988]. It was assumed that the flow of nitrogen was saturated with the vapor pressure of N₂O₅ based upon *Cantrell et al.* [1988]. The N₂O₅-doped nitrogen flow passed through nylon tubing in order to ensure that any heterogeneous decomposition of N₂O₅ into HNO₃ would remain on the walls and not in the gas phase. The temperature of the gas handling line was kept at 298 K, and therefore, about 1% thermal decomposition of N₂O₅ into NO₃ and NO₂ occurred [*Cantrell et al.*, 1988]. The residence time of N₂O₅ in the lines was approximately 30 s. The flow of N₂O₅-doped N₂ was diluted into 6000 sccm of zero air. Based on the vapor pressure and the flow rates, the concentration of N₂O₅ was 120 ppbv, while NO₂ and NO₃ were 1.2 ppbv. These experiments were also conducted under

wet and dry conditions, and no systematic differences were noted in either the ratio of the isotopically labeled $\text{H}^{15}\text{NO}_3\cdot\text{MSA}$ or ambient $\text{HNO}_3\cdot\text{MSA}$ signals.

Although NO , NO_2 , NO_3 , and N_2O_5 showed no observable interference in the $\text{MSA}\cdot\text{HNO}_3$ clusters under either wet or dry conditions, a significant change in sensitivity was observed with gas phase water. The vapor pressure of MSA is impacted by the relative humidity of water over the surface. Figure 3 shows the MSA ion counts for the monomer, dimer, trimer, and total counts of MSA versus relative humidity at 23°C. At low relative humidities, a high percentage of MSA is tied up in the trimer (and likely higher clusters), with relatively little MSA in the monomer. As the humidity increases, the number of trimers decreases, while the number of dimers significantly increases. At $\text{RH}=30\%$, the dimer population decreases, and at $\text{RH}=65\%$ the monomer becomes the dominant cluster. Overall, as the relative humidity increases, the vapor pressure of MSA decreases, and the cluster distribution moves toward the lower clusters. Therefore, one problem in using MSA reagent ion chemistry for HNO_3 detection is the changing sensitivity of the instrument as a function of ambient water vapor concentration. A more reliable way to introduce MSA and control its cluster distribution is needed, although the use of continual calibrations by the addition of H^{15}NO_3 helped to alleviate this problem.

Field studies. The NCAR CIMS HNO_3 instrument was flown on the NASA P3-B airplane as part of the NASA Transport and Chemical Evolution over the Pacific field experiment (TRACE-P) which took place February-April 2001 off the coast of eastern Asia (based in Hong Kong, PRC and Yokota Air Base, Japan). No data was collected during the transit flights 4-8 due to an ion source flooded with MSA vapor, which resulted in little or no ambient and calibration signals. Data from flight 9 was complicated by a lack of background and calibration signals resulting from large eddies removing both the isotopically-labeled calibration gas as well as the background zero air in the transport tube. The PFA cap shown in

HNO₃. Therefore, it was necessary to humidify the sheath flow to increase the monomer MSA ion. A fraction (0-1.4 sLpm) of ~ 3 sLpm sheath flow was bubbled through a 300 ml ~ 0.01 M aqueous sodium hydroxide (NaOH) solution to tie up any residual NO₃⁻ in the water (Aldrich, HPLC grade). The humidified flow was passed into an empty vessel to ensure that any small droplets would settle or collide with the container walls before entering the ion source. Finally, the sheath flow passed through a 0.9 micron nylon filter as well as a sodium bicarbonate (NaHCO₃) filter to remove any small (micron-sized) particles. The use of a humidified sheath flow was incrementally adjusted to keep the signal of the MSA dimer to approximately one-third of the monomer. At colder temperatures (<10°C ambient), a low dimer signal (due to lower vapor pressure of MSA) precluded the need for a humidified sheath flow.

Because the signal of the monomer ion of MSA changed with ambient conditions, the sensitivity of the HNO₃ signal (ion ratio m/e 158:m/e 95) changed depending upon ambient conditions. In the laboratory, sensitivities of the MSA-HNO₃ cluster were routinely 1-3 counts pptv⁻¹ s⁻¹. In contrast, in-flight operation of the instrument decreased the sensitivity by an order of magnitude relative to the laboratory experiments due to decreased gas flow into the vacuum system in order to accommodate the the other two channels - OH/MSA/H₂SO₄, HO₂/RO₂ and due to non-optimal pressures in the collision chamber (again, a compromise of the multi-channel shared vacuum housing). Although in-flight sensitivities of the cluster at times approached 1 ct pptv⁻¹ s⁻¹, more typical values were 0.1-0.4 cts pptv⁻¹ s⁻¹ during TRACE-P. Therefore, it was necessary to continuously calibrate with a flow of isotopically-labeled H¹⁵NO₃ at the top of the transport tube at all times.

Background estimates of HNO₃ sticking to instrument surfaces could be experimentally-determined by three different methods. The first method involved adding a large flow of zero air to the very top of the transport tube, just upstream from the addition of the calibration gas (not

shown in Figure 2 for clarity). Although this method worked reasonably on the ground, in-flight tests showed little effect even at zero air flows several sLpm greater than the flow down the transport tube. Because the transport tube lies perpendicular to the main flow in the large inlet, significant eddies formed in the upper region of the transport tube, and it is thought that large (though unquantified) amounts of the zero air were turbulently ejected from the inlet. Thus, this method was not used to estimate backgrounds while in-flight.

A second method involved overfilling the inlet with a flow of zero air just above the ion source. This method effectively examined the adsorption of HNO_3 to the metal pieces of the ion source, although it could not be used to estimate the amount of HNO_3 adsorbed to the extruded PFA upper transport tube. Figure 4 shows the responses of the ambient and calibration signals as zero air was added in front of the ion source during an 18 minute segment of Flight 16 (Yokota local #2) at an altitude of 17,500' (674 mb) while crossing the island of Japan. The signals have been normalized to their initial respective values when no zero air was being added. The zero point on the abscissa is the equivalence point where the amount of gas being drawn down the ion source is balanced by the flow of zero air above the ion source. Data below this point are considered "underfilling" the transport tube, while data above this is considered "overfilling" the transport tube.

In theory, the calibration signal should remain unchanged until the equivalence point. That is, the concentration of the calibration gas is independent of whether it is diluted by ambient air or by zero air. However, beyond the equivalence point when the inlet is overfilled, the flow of zero air through the transport tube is away from the ion source, and therefore, the concentration (and hence signal) of the calibration gas should be at background levels. For the case of the ambient signal, however, a flow of zero air decreases the amount of ambient air pulled into the ion source. Therefore, the response of the ambient signal should linearly depend

on the overfill flow. The theoretical curves for each case are shown in Figure 4 in dotted lines for the calibration and ambient signals.

In-situ field tests indicated that the responses of the signals differed from the expected behavior. Specifically, for the calibration gas, a sigmoid curve is observed – initially flat, showing no response as zero air is added and then rapidly decreasing when approaching within 2 sLpm of the equivalence point. No significant decrease in the signal was observed from slightly beyond the equivalence point to over 2 sLpm overfill. The calibration data suggests that turbulent eddies partially removed H^{15}NO_3 from the upper part of the transport when nearing the equivalence point. The data also show that overfilling the transport tube by greater than 2 sLpm of the equivalence flow was sufficient to record background conditions of calibration gas.

In contrast to the isotopically labeled H^{15}NO_3 , the response of the ambient signal more closely resembles the expected behavior. The measured signals were only slightly higher than the theoretical behavior. Not all of the zero air was drawn into the ion source when underfilling, but some small fraction was “pulled out” of the upper transport tube. Nonetheless, the amounts were quite small, and the general behavior was linear to first order. In addition, the ambient background was constant from the equivalence point to beyond 2 sLpm overfilling. Therefore, all backgrounds measured by flowing zero air above the ion source were done at overfills at least 2 sLpm beyond the equivalence point. Finally, the ambient concentration of HNO_3 may have changed during the in-flight test, and therefore, the results are potentially complicated by this factor. However, other chemical species such as NO_y , NO , O_3 , and CO indicated a relatively homogeneous air mass during the time of this test.

Similar tests like the one described above were conducted throughout TRACE-P. Data was entirely consistent with the results shown here, whether at low altitude (500' above sea level) or at high altitude (17,000'). A slight dependence was observed based on airspeed with

higher speeds having greater turbulence in the transport tube. For example, the sigmoid fit to the calibration curve in Figure 4 has a half-mean decay constant at -0.97 ± 0.05 sLpm with respect to equivalence at an airspeed of 297 knots. In contrast, speeds of 330 knots had -1.68 ± 0.03 sLpm while slower speeds of 274 knots had -0.94 ± 0.05 sLpm. Although pressure may indeed affect the degree of turbulence in the upper transport tube, the effect appeared to be caused by airspeed. A comparison of similar pressures (554, 516 mb) with different airspeeds (321, 308 knots, respectively) indicated slightly more turbulence (decay constants of -1.24 ± 0.13 vs 1.05 ± 0.15) with the higher airspeeds.

Figure 5a shows a representative background when overfilling the inlet with zero-air on Flight 14 (Okinawa to Yokota transit) at an altitude of 500'. The concentration of the calibration gas was 540 pptv while the average HNO_3 mixing ratio was ~ 470 pptv. Upon overfilling the inlet, both the ambient and calibration signals decreased to the same respective levels of < 0.005 ion ratio. In addition, the ambient HNO_3 data, with a temporal resolution of once every 5 seconds, shows that the background signal was achieved within the 5 s measurement time, and no significant decrease was observed for the duration of the overfill. Likewise, the signal responded within the 5 s measurement resolution when the overfilling was stopped. These results indicate that the background was a very small percentage of the overall signal, and that HNO_3 adsorbed to the metal surfaces of the ion source did not significantly affect the measurement.

Figure 5b shows a background of HNO_3 at much lower concentrations of ~ 80 pptv taken at 17,300' (509 mb, -9°C) on Flight 23 (Kona to Dryden transit). Like the previous example, the background ion ratios were ~ 0.005 . Despite the much closer difference in signal to background ion signal ratios and the relatively low concentration of HNO_3 , the response of the instrument to the background measurement remained rapid, on the timescale of the temporal resolution (5 s).

In addition, the overall background of the measurements indicated a limit of detection of ~ 5 pptv.

Finally, a third way to measure the background involved the removal of the calibration flow at the top of the upper transport tube. This method estimated the amount of HNO_3 adsorbed to the extruded PFA transport tube. Simply turning off the flow of the calibration gas was insufficient to test for a background as any small flows into the transport tube would still emit H^{15}NO_3 . Therefore, it was necessary to reverse the flow of the calibration gas by pumping on the calibration tube about one meter downstream of the end of the calibration tube. Figure 6 shows a representative example of the response of 515 pptv of the calibration signal upon pumping on the flow on Flight 14 at 14,300' (577 mb, -5°C). In the 20 s time resolution of the calibration measurement, the signal decreased to a value indistinguishable from the background level. The extruded PFA transport tube showed minimal wall/surface effects from the removal of calibration H^{15}NO_3 . However, because the inside surfaces of the long, thin tubing that carried the isotopically labeled H^{15}NO_3 flow had to re-equilibrate to a new concentration, relatively long periods of time (2-20 min) were needed to ensure the isotopic signal was stable again. Additionally, pumping on the calibration gas line pulled some amount of ambient HNO_3 into the calibration line. Thus, this background measurement was conducted only about once per flight, mainly to ensure that the extruded PFA transport tube remained a minimal sink for gas phase HNO_3 .

Although the background signal at masses 158 and 159 remained small throughout the field campaign, several factors contributed to its presence. Electronic noise ($< 1 \text{ ct s}^{-1}$) in the channeltron electron multiplier was determined by the signal at m/e 20 when the polarity of the quadrupole lenses was reversed. Desorption of HNO_3 off instrument surfaces and walls and any production of HNO_3 from the high energy ionization near the americium-241 were measured

through the tests noted above. The largest sources of background signals at masses 158 and 159 originated from isotopic contributions of significant peaks near m/e 156 and m/e 157. The m/e 156 and 157 peaks correlated with the availability of MSA reagent ions and thus were assumed to contain MSA. The remaining part of the cluster most likely resided at m/e 60 and m/e 61, CO_3^- and HCO_3^- , and indeed these species were abundant in mass spectra taken throughout the experiment. At concentrations of $\text{HNO}_3 < 100$ pptv, these peak signals were often larger (factor of 2-5) than the ambient signal. Although the resolution of the mass spectrometer was such that only around 1% of adjacent ions were measured ($m/\Delta m=320$), the isotopic abundances of the likely elements - sulfur ($^{33}\text{S}=0.76\%$, $^{34}\text{S}=4.22\%$), carbon ($^{13}\text{C}=1.11\%$), oxygen ($^{17}\text{O}=0.037\%$, $^{18}\text{O}=0.204\%$), and nitrogen ($^{15}\text{N}=0.37\%$) - resulted in significant mass counts at the ambient and calibration signals (m/e = 158, 159). The signals at m/e 156 and m/e 157 were measured every 20 s during portions of several flights and no obvious dependence on sheath flow, pinhole flow, or zero air was observed. In addition, on all flights these species were measured at least once every 10 minutes during partial but continual mass scans as part of the measurement scheme. No apparent correlation was observed with any factor besides increasing or decreasing with MSA monomer abundance. It remains unclear how or why these species would cluster so readily with MSA or be so abundant in the ion source, but they most likely form before MSA ions are introduced.

Additional background contributions at the ambient signal derived from signals from adjacent masses (1%) and the impurity of the H^{15}NO_3 calibration source (0.6%). In total, the m/e 158 signal had contributions from the following sources:

$$\text{measured m/e 158 signal} = 5.4\%(v) + 4.24\%(w) + x + 1.4\%(y) + 0\%(z)$$

where v, w, x, y, and z correspond to the “real” signals (effects of isotopes removed, adjacent masses removed, etc.) at masses 156, 157, 158, 159, and 160 signals, respectively. A linear set of

equations for each of the five masses was solved taking into account all of these factors on one another. Generally, the size of this correction was small (< 10%) for the ambient signal at mixing ratios > 100 pptv HNO₃ but became increasingly significant at lower mixing ratios. Ultimately, the correction for the relatively large peaks at m/e 156 and m/e 157 accounted for most of the background in the lower concentration data and was the single largest source of error in the measurements at low (< 100 pptv) concentrations. Overall error ($\pm 2\sigma$) of the measurement including systematic and random errors were the limit of detection (5 pptv) plus the following: $\pm 25\%$ pptv at mixing ratios < 100 pptv, $\pm 20\%$ from 100-200 pptv, and $\pm 15\%$ for mixing ratios > 200 pptv.

Calibrations of the system occurred by the addition of the isotopically labeled H¹⁵NO₃ in the transport tube. The H¹⁵NO₃ source contained 99.6% enrichment of 15N-nitric acid and was enclosed in a permeation tube (Vici). The tube was initially reported with an emission rate of 57 ng min⁻¹, however permeation tubes are notorious for different emission rates under different conditions [Talbot *et al.*, 1997; Ryerson *et al.*, 1999]. Therefore, the permeation tube was held in a heated cavity with a critical orifice of 7 cm of 0.06 mm i.d. PFA tubing. The permeation tube was always kept at a constant pressure of 35 psi N₂ during the mission (except when changing tanks). An inert flow meter (Teflon internal surfaces) upstream of the permeation tube measured the flow (~ 100 sccm), and the pressure over the tube was regulated to 35 psi. In this way, N₂ was continually flowing over the permeation source at a constant pressure even when the aircraft had no power. Finally, the flow over the permeation cell passed through a manifold where a portion (0-100 sccm) of the flow could be removed by pumping, while the remaining amount joined a carrier flow of ~ 100 sccm N₂. The carrier/calibration flow passed through ~ 40 cm of 1.1 mm o.d., 0.6 mm i.d. PFA tubing. The carrier/calibration tubing was enclosed by 1.3 mm i.d.

stainless steel tubing which was resistively heated to 45°C from just inside the fuselage to the outside edge of the transport tube.

Temperature control of the permeation tube consisted of an aluminum thermofoil backed, resistive heater (Minco) and a temperature controller (Watlow, model 241). The permeation tube was kept at a constant temperature of 40°C except when the airplane was powered down. Before flight, the temperature of the permeation cell was raised to 40°C at least 2 hours before measurements commenced. Ground-based tests indicated that one hour was sufficient for the tubing walls to re-equilibrate to a new permeation rate and subsequent changes in H¹⁵NO₃ concentration. The mass of the permeation cell was measured for eight months after the end of the deployment, and a constant emission rate of 33.5 ± 1.3 ng min⁻¹ was obtained as shown in Figure 7. Although no mass measurements were made in the field, the output of the permeation cell was measured twice in the field by the University of New Hampshire mist chamber/ion chromatography instrument on the NASA DC-8 airplane. The UNH measurements yielded an average of 29 ± 1 ng min⁻¹ for three measurements before P-3B flight 17, and 32 ± 2 ng min⁻¹ for two measurements before P-3B flight 23. The mass data and the two ion chromatography measurements agreed to within 15%, and it provides strong evidence that the permeation cell emitted H¹⁵NO₃ at a rate near 33.5 ng min⁻¹ during the entire TRACE-P campaign. The overall accuracy of the permeation cell calibration was the largest source of error for measurements above 200 pptv.

Multipoint calibrations were conducted in-flight to examine the linearity and response of the measured H¹⁵NO₃ signal versus H¹⁵NO₃ concentration. Typically, multipoint calibrations were conducted at least once per flight for flights 16-24. To conduct these experiments, a known amount of the calibration gas was removed before flowing into the inlet. A representative example of an in-flight calibration is shown in Figure 8 for a wide range of altitudes and mixing

ratios (50-2500 pptv) during Flight 16 (Yokota local #2). Despite the much different environments of the data (ranging from 17,000 feet to the marine boundary layer), a linear response is clearly noted in the data in Figure 8, suggesting that the continuous single-point calibrations throughout the rest of the flight were valid. Although the absolute calibration factor and sensitivity did change from flight to flight and within a flight (mainly due to the impact of MSA clustering on the availability of MSA monomer as noted previously), the overall sensitivity was generally around 2000-3000 pptv/ion ratio.

Intercomparisons. Three brief and informal intercomparisons between instruments onboard the NASA P-3B and NASA DC-8 were conducted during TRACE-P. Typical distances between the airplanes ranged from 0.2-1.0 km with a vertical separation of less than 100 m. For more information on the intercomparisons, refer to *Eisele et al.* (this issue). During the first intercomparison on the transit to Hong Kong, no data were obtained due to a lack of reagent ion signal and calibration signal (MSA had coated the ion source and reagent monomer MSA signals were extremely small). NCAR CIMS recorded no data on the second (P3 flight #16, DC flight #10) and third (P3-flight #23, DC flight #20) intercomparisons, and the results were compared to the HNO_3 measurements from the mist chamber/ion chromatograph instrument from the University of New Hampshire onboard the DC-8 aircraft (UNH). Details of the UNH instrument are described elsewhere (*Talbot et al., 1997, 1999, this issue*). It should be noted that each instrument detected HNO_3 with a different technique (chemical ionization versus ion chromatography), vastly different inlets, and independent permeation standards (though as noted above, within 15% of one another).

Figure 9a shows the data collected on the second intercomparison, lasting about 24 minutes at 17,000'. No data was collected in the final 3 minutes of the intercomparison from NCAR CIMS due to turbulence issues arising from an overflow flow near the equivalence point.

The light blue solid line shows the NCAR CIMS HNO_3 data collected every 5 seconds. The red line shows the UNH measurements. Finally, the dark blue line shows the NCAR CIMS measurements averaged within the UNH sampling window. Reasonable agreement is observed between measurements with NCAR CIMS reporting an average of 158 ± 32 pptv ($N=224$, 1σ) in 5 s measurements compared to 185 ± 28 pptv ($N=9$) for the UNH samples of 120-180 s. The averages were within the error bars of $\pm 20\%$ for NCAR and $\pm 15\%$ for UNH. On a point by point basis, CIMS was lower than UNH on 6 of 9 points, with a mean deviation of UNH greater than NCAR by 23 pptv and a standard deviation of the mean of 29 pptv. It is unclear why three data points lie outside of each other's error bars or why NCAR had lower measurements than UNH, and potential sources of disagreements are noted later.

Figure 9b shows the results of the third intercomparison over the Pacific Ocean just east of Hawaii. This intercomparison consisted of 20 minutes at 17,000', followed by a descent at 500' per minute to 500', and 20 minutes at 500'. A problem with electrical noise in the OH channel of the four channel system prevented data collection for a 7 minute period on the descent for NCAR CIMS. Both techniques measured low values of HNO_3 during the high-altitude portion. CIMS measured on average 12 pptv higher than UNH during the high-altitude portion, with the exception of a spike measured only by UNH around 18:24 UT. On the descent, both techniques measured a local maximum of 190 pptv HNO_3 around 10,000 feet and subsequent decrease to < 100 pptv near the end of the descent. A gradual rise of HNO_3 was measured by both instruments during the boundary layer run. A significant deviation between the datasets did appear near the end of the boundary layer run with CIMS HNO_3 measuring 72 pptv higher than the values obtained by UNH. No other tracers identified significant deviations, and therefore, a change in air mass is not likely a valid reason for the discrepancy. Overall, the mean deviation

between the measurements indicates that CIMS was 15 pptv higher than UNH throughout the intercomparison.

One potential reason for the discrepancies between the two measurements is the sampling of nitrate-containing particles ($< 2.5 \mu\text{m}$ aerodynamic diameter) by UNH's instrument. The NCAR CIMS inlet was not expected to directly sample particles because only gas phase ions (not charged particles) were electrostatically directed into the vacuum system. Sampling of nitrate-containing particles would result in higher measurements of gas phase HNO_3 relative to the true amount. Particulate nitrate smaller than $1.3 \mu\text{m}$ diameter was measured onboard the P-3B [Ma *et al.*, *this issue*; Weber *et al.*, 2001]. The second intercomparison showed steadily increasing levels of particulate nitrate from 22 to 44 pptv, and UNH measurements indeed averaged 27 pptv higher than NCAR CIMS. Particulate nitrate on the third intercomparison were generally below 20 pptv, and yet NCAR CIMS reported higher measurements than UNH. Therefore, the differences between the HNO_3 measurements could not be explained by the amount of particulate nitrate measured onboard the P-3B. A more thorough analysis on the size distributions of nitrate-containing aerosol particles is ultimately needed to quantify how the sampling of particulate nitrate may impact HNO_3 measurements.

Figure 10 shows a plot of the NCAR measurements versus UNH measurements for all of the datapoints in the second and third intercomparisons. The associated error bars for the measurements are determined using the stated errors mentioned previously for NCAR CIMS and the uncertainties of UNH stated in the TRACE-P data archive: $\pm 30\%$ for < 20 pptv, $\pm 25\%$ for 20-25 pptv, $\pm 20\%$ for 25-100 pptv, and $\pm 15\%$ for > 100 pptv. The uncertainties of each measurement technique for the data in Fig. 10 differ from the more general ones used by Eisele *et al.* [this issue]. The error limits shown in Figure 10 are the square root of the sum of the errors squared for each measurement. The slope of the data is 0.94 ± 0.18 (2σ), showing general

agreement between techniques, although an offset of 19 ± 14 pptv (2σ) indicates that potential disagreements may be related to background issues. Overall, 29 out of the 40 datapoints lie within the expected error bars of each set of measurements, and 8 of the 11 discrepancies lie at mixing ratios below 100 pptv. Clearly, the two techniques appear to be in good agreement, although issues such as background determinations and aerosol particle sampling most likely need to be better quantified, especially at low mixing ratios.

Finally, the response of the inlet and instrument to rapid changes in ambient HNO_3 concentration is demonstrated. Figure 11a shows the response of the instrument to ship plumes at 500' above the South China Sea on Flight 14 (Okinawa to Yokota transit). A uniform atmospheric concentration of ~ 450 pptv prevailed, although individual spikes as high as 1800 pptv occurred during the 5 s measurement resolution time for this flight. In addition, multiple decreases and increases occurred, showing that the ability of the inlet to resolve rapid HNO_3 changes and also return to baseline values. If significant amounts of HNO_3 had been adsorbed onto the inlet (e.g. if the "true" value of the peaks were 5 ppbv), one would expect to observe desorption of HNO_3 off the inlet surfaces with corresponding increases in the atmospheric background level of ~ 450 pptv during this time. For comparison, the corresponding changes for NO_y (1 s resolution) as measured by the University of Tokyo are also shown (*Kondo et al., 1997; Koike et al., 2000; Miyazaki et al., this issue*). Tight correlation is observed, indicating very good resolution of the inlet. No attempts have been made to resolve the ~ 3 s offset between the measurements. Figure 11b shows a vertical profile of HNO_3 during descent into the marine boundary layer where highly polluted air was encountered. Upon entering the polluted layer, ambient HNO_3 increases from around 360 pptv to 1600 pptv in 15 s. The rapid changes presented in Figure 11, in combination with in-flight tests of the calibration gas, suggest that

HNO₃ adsorption onto inlet surfaces was not a significant problem and therefore generally did not interfere with the measurement.

Summary and future work. Nitric acid was detected using a unique choice of inlet design and materials and selective ion chemical ionization mass spectrometry using methanesulfonic acid as a reagent ion. The instrument measured HNO₃ every 5 s with a limit of detection of 5 pptv. The inlet was not actively heated to prevent possible desorption of particulate nitrates into gas phase HNO₃. The instrument was calibrated continuously using isotopically labeled H¹⁵NO₃, and the inlet demonstrated very few problems of surface adsorption. Intercomparisons with a more established HNO₃ measurement technique by UNH were promising.

Future areas of improvement with this instrument include identifying a more reliable way to introduce methanesulfonic acid or selecting a more stable reagent ion. Under low concentrations of reagent ion, the sensitivity of the measurement decreased significantly. One possibility to better control MSA reagent concentration includes using a reduced pressure ion source with extruded PFA surfaces. Although MSA worked favorably for this campaign, future research will examine ways to control the addition of MSA to the ion source (as opposed to manually placing MSA droplets in the ion source). Furthermore, the presence of unknown peaks at m/e 156 and m/e 157 can significantly deplete the availability of reagent ion MSA, and solving this problem will enhance the sensitivity of the technique. Nonetheless, the techniques described here are a start toward quantifying and ultimately better understanding the chemistry of HNO₃ in the troposphere.

Acknowledgements. MAZ gratefully acknowledges support from an NCAR ASP Postdoctoral Fellowship. The authors thank J. Dibb, E. Scheuer, and R. Talbot for invaluable assistance and

advice in the calibration of the permeation standard and for great cooperation in the intercomparisons. We also thank J. Orlando and G. Tyndall for the use of their N₂O₅, J. Fox and the ATD instrument shop for inlet design and construction, J. Vanderpol for shop work, T. Ryerson of the NOAA AL for permeation cell oven plans, and R. Hendershot and W. Bradley for electronics assistance. Finally, all of this work would not have happened without the helpful assistance of the NASA TRACE-P Science Team and aircraft support personnel at NASA Wallops Flight Facility. The National Center for Atmospheric Research is operated by the University Corporation for Atmospheric Research under sponsorship of the National Science Foundation.

References

- Abbatt, J.P.D., "Interaction of HNO₃ with water-ice surfaces at temperatures of the free troposphere", *Geophys. Res. Lett.*, *24*, 1479-1482, 1997.
- Adams, P.J., J.H. Seinfeld, and D.M. Koch, "Global concentrations of tropospheric sulfate, nitrate, and ammonium aerosol simulated in a general circulation model", *J. Geophys. Res.*, *104*, 13791-13823, 1999.
- Arnold, F., J. Scheid, T. Stilp, H. Schlager, and M.E. Reinhardt, "Measurements of jet aircraft emissions at cruise altitude I: the odd-nitrogen gases NO, NO₂, HNO₂, and HNO₃", *Geophys. Res. Lett.*, *12*, 2421-2424, 1992.
- Ayers, G.P., R.W. Gillett, and J.L. Gras, "On the vapor pressure of sulfuric acid", *Geophys. Res. Lett.*, *7*, 433-436, 1980.
- Christopher A. Cantrell, G. D. Edwards, S. Stephens, R. L. Mauldin, M. Zondlo, E. Kosciuch, F. L. Eisele, R. E. Shetter, B. L. Lefer, S. Hall, F. Flocke, A. Weinheimer, A. Fried, E. Apel, Y. Kondo, D. R. Blake, N. Blake, I. Simpson, A. Bandy, D. Thornton, B. Heikes, H. Singh, W. Brune, H. Harder, M. Martinez-Harder, M. A. Avery, S. Vay, J. D. Barrick, G. W. Sachse, J. R. Olsen, J. H. Crawford, "Peroxy Radical Behavior during TRACE-P as Measured Aboard the NASA P-3B Aircraft", submitted to the TRACE-P special issue, *J. Geophys. Res.*, 2002.
- Cantrell, C.A., J.A. Davidson, A.H. McDaniel, R.E. Shetter, and J.G. Calvert, "The equilibrium constant for N₂O₅ ⇌ NO₂ + NO₃: absolute determination by direct measurement from 243-273 K", *J. Chem. Phys.*, *88*, 4997-5006, 1988.
- Davidson, J.A., A.A. Viggiano, C.J. Howard, I. Dotan, F.C. Fehsenfeld, D.L. Albritton, and E.E. Ferguson, "Rate constants for the reactions of O₂⁺, NO₂⁺, NO⁺, H₃O⁺, CO₃⁻, NO₂⁻, and halide ions with N₂O₅ at 300 K", *J. Chem. Phys.*, *68*, 2085-2087, 1978.
- Dentener, F.J., G.R. Carmichael, Y. Zhang, J. Lelieveld, and P.J. Crutzen, "Role of mineral aerosol as a reactive surface in the global troposphere", *J. Geophys. Res.*, *101*, 22869-22889, 1996.
- Eisele, F.L., R.L. Mauldin, D.J. Tanner, J.R. Fox, T. Mouch, and T. Scully, "An inlet/sampling duct for airborne OH and sulfuric acid measurements", *J. Geophys. Res.*, *102*, 27993-28001, 1997.
- Eisele, F.L., L. Mauldin, C. Cantrell, M. Zondlo, E. Apel, A. Fried, J. Walega, R. Shetter, B. Lefer, F. Flocke, A. Weinheimer, M. Avery, S. Vay, G. Sachse, H.B. Singh, W. Brune, H. Harder, M. Martinez, A. Bandy, D. Thornton, B. Heikes, Y. Kondo, D. Riemer, S. Sandholm, D. Tan, R. Talbot, and J. Dibb, "Summary of measurement intercomparisons during TRACE-P", submitted to the TRACE-P Special Issue, *J. Geophys. Res.*

- Jacob, D.J., B. Heikes, S.-M. Fan, J.A. Logan, D.L. Mauzerall, J.D. Bradshaw, H.B. Singh, G.L. Gregory, R.W. Talbot, D.R. Blake, G.W. Sachse, "Origin of ozone and NO_x in the tropical troposphere: a photochemical analysis of aircraft observations over the South Atlantic basin", *J. Geophys. Res.*, *101*, 24235-24250, 1996.
- Kerminen, V.-M., A.S. Wexler, and S. Potukuchi, "Growth of freshly nucleated particles in the troposphere: roles of NH₃, H₂SO₄, HNO₃, and HCl", *J. Geophys. Res.*, *102*, 3715-3724, 1997.
- Kondo, Y., S. Kawakami, M. Koike, D.W. Fahey, H. Nakajima, Y. Zhao, N. Toriyama, M. Kanada, G.W. Sachse, and G.L. Gregory, "The performance of an aircraft instrument for the measurement of NO_y", *J. Geophys. Res.*, *102*, 28663-28671, 1997.
- Koike, M., Y. Kondo, G.L. Gregory, B.E. Anderson, G.W. Sachse, D. Blake, H.B. Singh, A. Thompson, K. Kita, Y. Zhao, T. Sugita, R. Shetter, H. Ikeda, S.C. Liu, L. Jeagle, and N. Toriyama, "Impact of aircraft emissions on reactive nitrogen over the North Atlantic Flight Corridor region", *J. Geophys. Res.*, *105*, 3665-3677, 2000.
- Koppel, I.A., R.W. Taft, F.A. Anvia, S.-Z. Zhu, L.-Q. Hu, K.-S. Sung, D.D. DesMarreau, L.M. Yagupolskii, Y.L. Yagupolskii, N.V. Ignat'ev, N.V. Kondratenko, A.Y. Volkonskii, V.M. Vlasov, R. Notario, and P.-C. Mari, "The gas-phase acidities of very strong neutral bronsted acids", *J. Am. Chem. Soc.*, *116*, 3047-3057, 1994.
- Laaksonen, A., J. Hienola, and M. Kulmala, "Supercooled cirrus cloud formation modified by nitric acid pollution of the upper troposphere", *Geophys. Res. Lett.*, *24*, 3009-3012, 1997.
- Liang, J., L.W. Horowitz, D.J. Jacob, Y. Wang, A.M. Fiore, J.A. Logan, G.M. Gardner, and J.W. Munger, "Seasonal budgets of reactive nitrogen species and ozone over the United States, and export fluxes to the global atmosphere", *J. Geophys. Res.*, *103*, 13435-13450, 1998.
- Lin, J.-S., and A. Tabazadeh, "The effect of nitric acid uptake on the deliquescence and efflorescence of binary ammoniated salts in the upper troposphere", *Geophys. Res. Lett.*, *10.1029/2002GL015251*, 2002.
- Ma, Y., R.J. Weber, Y.-N. Lee, D.C. Thornton, A.R. Bandy, A.D. Clarke, D.R. Blake, G.W. Sachse, H.E. Fuelberg, C.M. Kiley, J.-H. Woo, D.G. Streets, G.R. Carmichael, F.L. Eisele, "The Characteristics and Influence of Biomass Burning Aerosols on Fine Particle Ionic Composition Measured in Asian Outflow During TRACE-P", submitted to the TRACE-P special issue, *J. Geophys. Res.*
- Mauldin, R.L., D.J. Tanner, and F.L. Eisele, "Measurements of OH during PEM-Tropics A", *J. Geophys. Res.*, *104*, 5817-5827, 1999.
- Mauldin, R.L., G.J. Frost, G. Chen, D.J. Tanner, A.S.H. Prevot, D.D. Davis, and F.L. Eisele, "OH measurements during the First Aerosol Characterization Experiment (ACE 1): observations and model comparisons", *J. Geophys. Res.*, *103*, 16713-16729, 1998a.

- Mauldin, R.L., D.J. Tanner, and F.L. Eisele, "A new chemical ionization mass spectrometer technique for the fast measurement of gas phase nitric acid in the atmosphere", *J. Geophys. Res.*, *103*, 3361-3367, 1998b.
- McDaniel, A.H., J.A. Davidson, C.A. Cantrell, R.E. Shetter, and J.G. Calvert, "Enthalpies of formation of dinitrogen pentoxide and the nitrate free radical", *J. Phys. Chem.*, *92*, 4172-4175, 1988.
- Meng, Z., D. Dabdub, and J.H. Seinfeld, "Chemical coupling between atmospheric ozone and particulate matter", *Science*, *277*, 116-119, 1997.
- Miller, T.M., J.O. Ballenthin, R.F. Meads, D.E. Hunton, W.F. Thorn, and A.A. Viggiano, "Chemical ionization mass spectrometer technique for the measurement of HNO₃ in air traffic corridors in the upper troposphere during the SONEX campaign", *J. Geophys. Res.*, *105*, 3701-3707, 2000.
- Möhler, O. and F. Arnold, "Flow reactor and triple quadrupole mass spectrometer investigations involving nitric acid: implications for atmospheric HNO₃ detection by chemical ionization mass spectrometry", *J. Atmos. Chem.*, *13*, 33-61, 1991.
- Miyazaki, Y., Y. Kondo, M. Koike, K. Kita, N. Takegawa, H. E. Fuelberg, G. W. Sachse, F. Flocke, A. J. Weinheimer, H. B. Singh, M. Zondlo, R. W. Talbot, S. T. Sandholm, M. A. Avery, and D. R. Blake, "Synoptic-scale transport of reactive nitrogen over the western Pacific in spring", submitted to the TRACE-P Special Issue, *J. Geophys. Res.*
- Neuman, J.A., L.G. Huey, R.W. Dissly, F.C. Fehsenfeld, F. Flocke, J.C. Holecek, J.S. Holloway, G. Hubler, R. Jakoubek, D.K. Nicks Jr., D.D. Parrish, T.B. Ryerson, D.T. Sueper, and A.J. Weinheimer, "Fast-response airborne in situ measurements of HNO₃ during the Texas 2000 Air Quality Study", *J. Geophys. Res.*, doi:10.1029/2001JD001437, 2002.
- Neuman, J.A., R.S. Gao, M.E. Schein, S.J. Ciciora, J.C. Holecek, T.L. Thompson, R.H. Winkler, R.J. McLaughlin, M.J. Northway, E.C. Richard, and D.W. Fahey, "A fast-response chemical ionization mass spectrometer for in situ measurements of HNO₃ in the upper troposphere and lower stratosphere", *Rev. Sci. Instrum.*, *71*, 3886-3894, 2000.
- Neuman, J.A., L.G. Huey, T.B. Ryerson, and D.W. Fahey, "Study of inlet materials for sampling atmospheric nitric acid", *Envi. Sci. Tech.*, *33*, 1133-1136, 1999.
- Reiner, T., O. Mohler, and F. Arnold, "Improved atmospheric trace gas measurements with an aircraft-based tandem mass spectrometer: Ion identification by mass-selected fragmentation studies", *J. Geophys. Res.*, *103*, 31309-31320, 1998.
- Ryerson, T.B., L.G. Huey, K. Knapp, J.A. Neuman, D.D. Parrish, D.T. Sueper, and F.C. Fehsenfeld, "Design and initial characterization of an inlet for gas-phase NO_y measurements from aircraft", *J. Geophys. Res.*, *104*, 5483-5492, 1999.

- Schneider, J., F. Arnold, V. Burger, B. Droste-Franke, F. Grimm, G. Kirchner, M. Klemm, T. Stilp, K.-H. Wohlfrom, "Nitric acid (HNO₃) in the upper troposphere and lower stratosphere at midlatitudes: new results from aircraft-based mass spectrometric measurements", *J. Geophys. Res.*, *103*, 25337-25343, 1998.
- Singh, H.B., D. Herlth, R. Kolyer, L. Salas, J.D. Bradshaw, S.T. Sandholm, D.D. Davis, J. Crawford, Y. Kondo, M. Koike, R. Talbot, G.L. Gregory, G.W. Sachse, E. Browell, D.R. Blake, F.S. Rowland, R. Newell, J. Merrill, B. Heikes, S.C. Liu, P.J. Crutzen, M. Kanakidou, "Reactive nitrogen and ozone over the western Pacific: distribution, partitioning, and sources", *J. Geophys. Res.*, *101*, 1793-1808, 1996.
- Singh, H.B., W. Viezee, Y. Chen, A.N. Thakur, Y. Kondo, R.W. Talbot, G.L. Gregory, G.W. Sachse, D.R. Blake, J.D. Bradshaw, Y. Wang, and D.J. Jacob, "Latitudinal distribution of reactive nitrogen in the free troposphere over the Pacific Ocean in late winter/early spring", *J. Geophys. Res.*, *103*, 28237-28246, 1998.
- Talbot, R.W., J.E. Dibb, B.L. Lefer, E.M. Scheuer, J.D. Bradshaw, S.T. Sandholm, S. Smyth, D.R. Blake, N.J. Blake, G.W. Sachse, J.E. Collins, and G.L. Gregory, "Large-scale distributions of tropospheric nitric, formic, and acetic acids over the western Pacific basin during wintertime", *J. Geophys. Res.*, *102*, 28203-28313, 1997.
- Talbot, R.W., J.E. Dibb, E.M. Scheuer, D.R. Blake, N.J. Blake, G.L. Gregory, G.W. Sachse, J.D. Bradshaw, S.T. Sandholm, and H.B. Singh, "Influence of biomass combustion emissions on the distribution of acidic trace gases over the southern Pacific basin during austral springtime", *J. Geophys. Res.*, *104*, 5623-5634, 1999.
- Talbot, R., J. Dibb, E. Scheuer, G. Seid, R. Russo, S. Sandholm, D. Tan, H. Singh, D. Blake, N. Blake, E. Atlas, G. Sachse, and M. Avery, "Reactive nitrogen in Asian continental outflow over the western Pacific: results from the NASA TRACE-P Airborne mission", submitted to the TRACE-P special issue, *J. Geophys. Res.*
- Tang, I.N., and H.R. Munkelwitz, "Determination of vapor pressure from droplet evaporation kinetics", *J. Coll. and Int. Sci.*, *141*, 109-118, 1991.
- Tanner, D.J., and F.L. Eisele, "Present OH measurement limits and uncertainties", *J. Geophys. Res.*, *100*, 2883-2892, 1995.
- Underwood, G.M., C.H. Song, M. Phadnis, G.R. Carmichael, and V.H. Grassian, "Heterogeneous reactions of NO₂ and HNO₃ on oxides and mineral dust: a combined laboratory and modeling study", *J. Geophys. Res.*, *106*, 18055-18066, 2001.
- Weber, R.J., D. Orsini, Y. Daun, Y.-N. Lee, P.J. Klotz, and F. Brechtel, "A particle-into-liquid collector for rapid measurement of aerosol bulk chemical composition", *Aerosol Sci. Tech.*, *35*, 718-727, 2001.

Zondlo, M.A., S.B. Barone, and M.A. Tolbert, "Uptake of HNO₃ on ice under upper tropospheric conditions", *Geophys. Res. Lett.*, 24, 1391-1394, 1997.

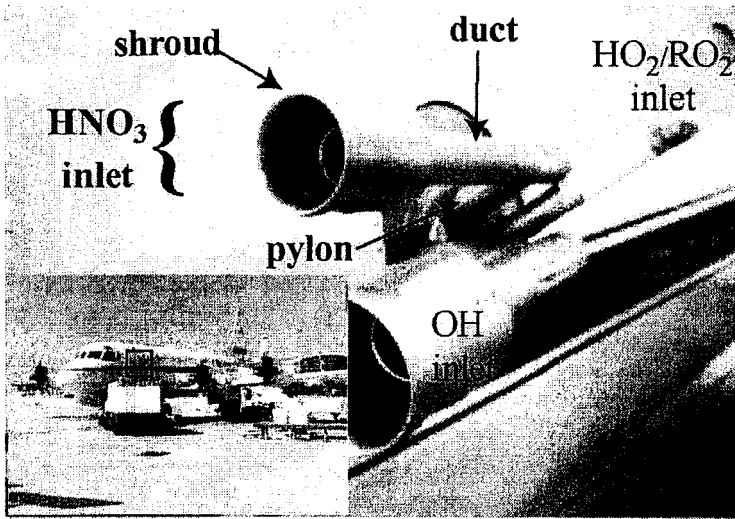


Figure 1. Photograph of the HNO_3 inlet showing the shroud, duct, and pylon. Also marked are the $\text{OH}/\text{H}_2\text{SO}_4/\text{MSA}$ inlet as well as the HO_2/RO_2 inlet. The inlets are located on the front, port side of the P-3B aircraft shown in the box in the lower left inset.

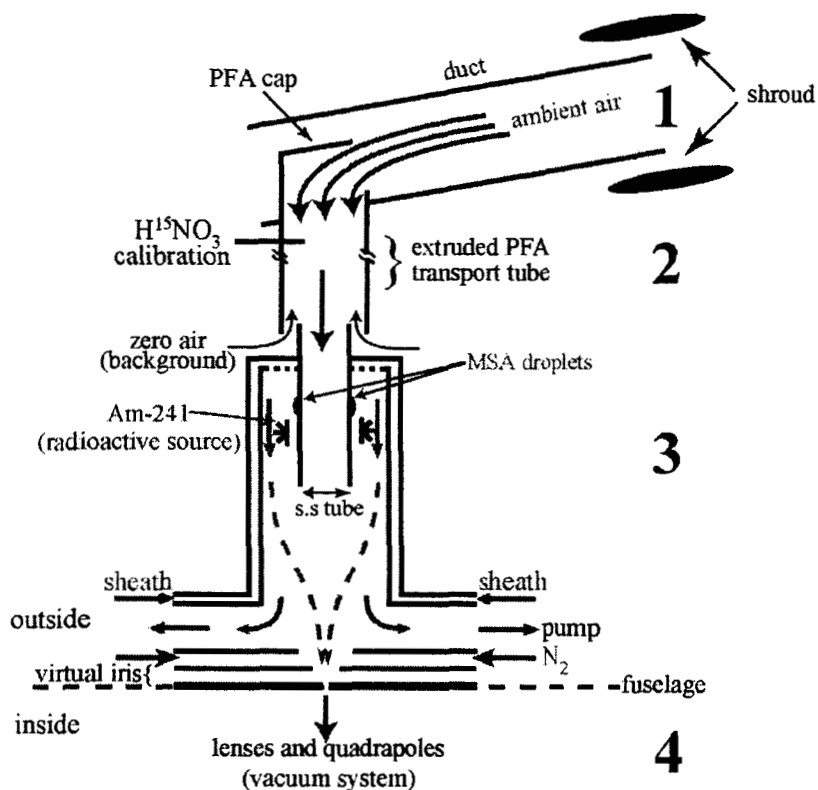


Figure 2. Schematic of the inlet and ion source showing the duct (1), transport tube (2), ion source (3), and vacuum system (4). A sample of ambient air is pulled toward the extruded PFA transport tube where isotopically-labeled ^{15}N nitric acid is added for calibration. The ambient air continues through a stainless steel tube into the ion source where ion-molecule reactions occur. MSA ions are generated when the sheath flow of zero air draws the vapor off tiny MSA droplets and passes over the $Am-241$ foil. Ions meet the ambient air and are then directed through a flow of dry nitrogen before entering the virtual iris and finally the vacuum system. Backgrounds were determined by flowing zero air immediately above the ion source and by removing the flow of the calibration gas.

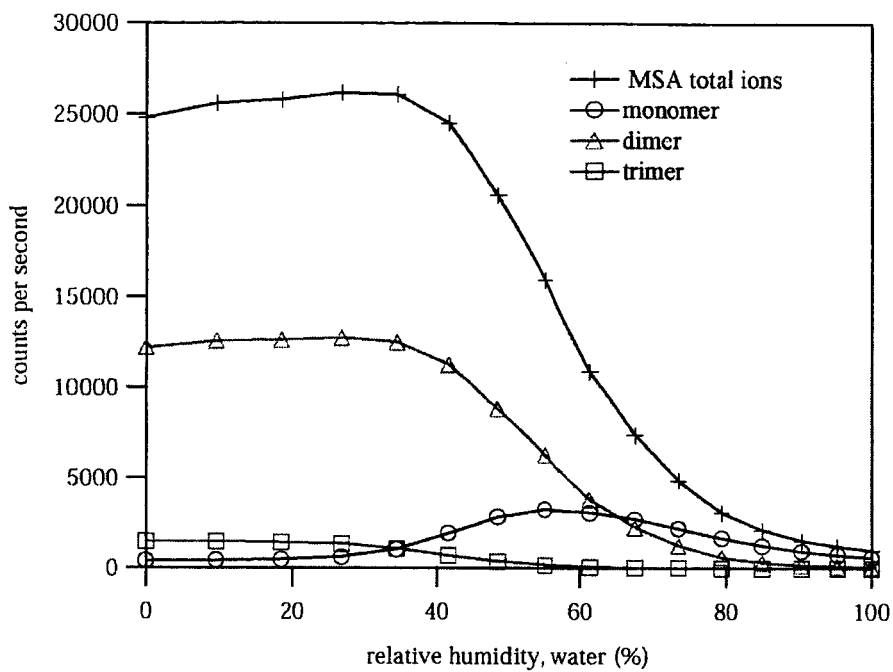


Figure 3. Plot of the populations of monomer (○, $m/e=95$), dimer (Δ, $m/e 191$), and trimer (□, $m/e 287$) clusters of MSA ions as a function of relative humidity at 23°C. The total number of MSA species detected (+, $= 3*\text{trimer}+2*\text{dimer}+\text{monomer}$) decreases dramatically as the humidity increases, while the dominant cluster size shifts towards the monomer.

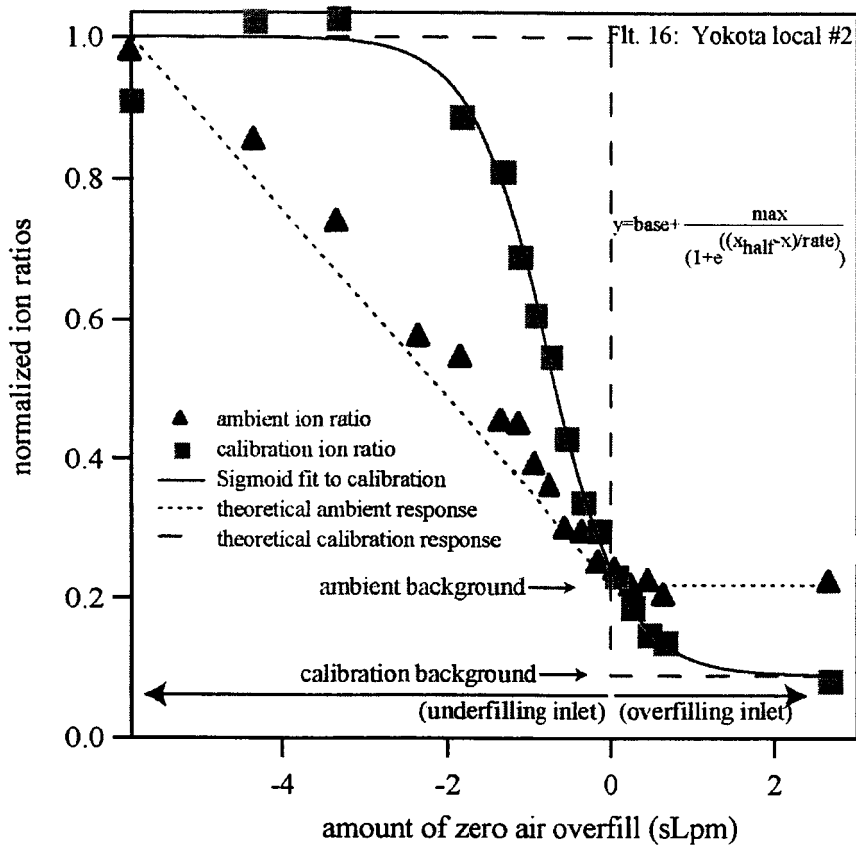


Figure 4. Response of the ambient and calibration signals upon adding a flow of zero air directly above the ion source from 5:13-5:31 UT on Flight 16 at an airspeed of 297 knots at 674 mb. The mean ambient mixing ratio was 83 pptv and the mean calibration mixing ratio was 245 pptv. The equivalence point of 0 sLpm is where the flow into the ion source equals the flow of zero air above it. Neglecting turbulence, the expected responses of the ambient and calibration signals are shown as dashed lines. Both signals were normalized to unity for comparison purposes. Fit parameters for the calibration ($\pm 1s$): base = 1.00 ± 0.02 , max = -0.91 ± 0.04 , xhalf = -0.77 ± 0.05 , rate = 0.48 ± 0.05 .

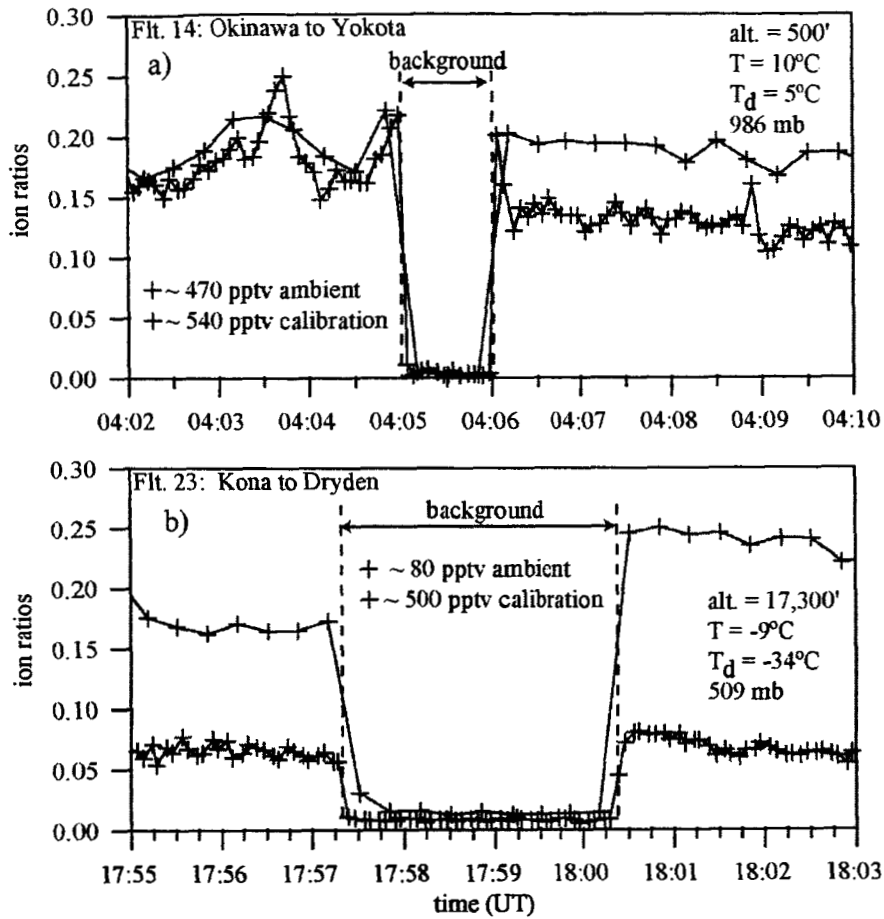


Figure 5. The response of the ambient (5 s resolution) and calibration signals (20 s resolution) upon flowing zero air in front of the ion source: (a) 500' on Flight 14 and (b) 17,300' on Flight 23. Background signals were attained within the 5 s resolution of the measurements.

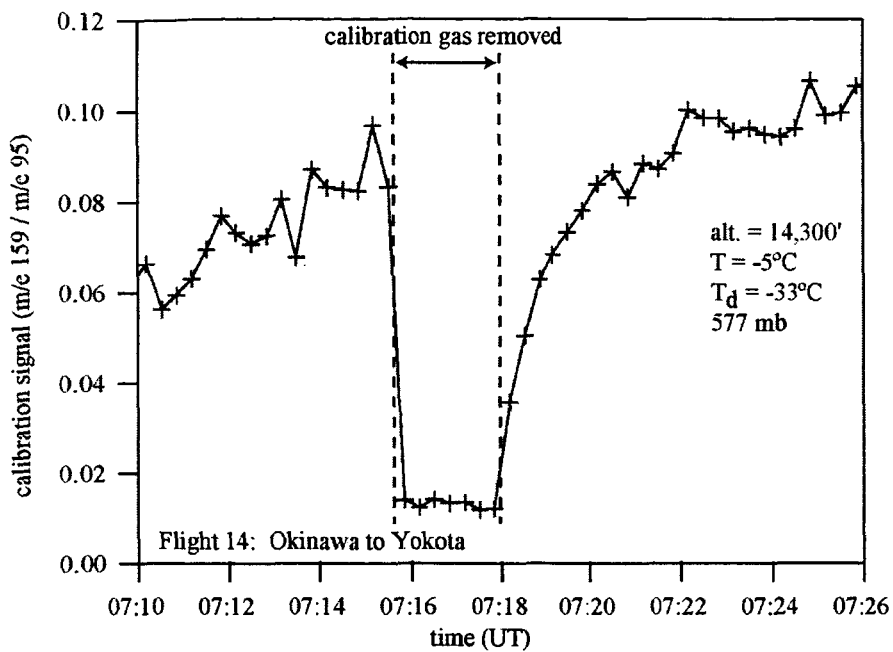


Figure 6. Response of the calibration signal when a flow of 515 pptv H^{15}NO_3 is removed from the inlet. A rapid ($< 20\text{s}$) drop to a constant, background value is observed. The gradual recovery of the signal results from re-equilibration of the H^{15}NO_3 concentration within the carrier flow tubing.

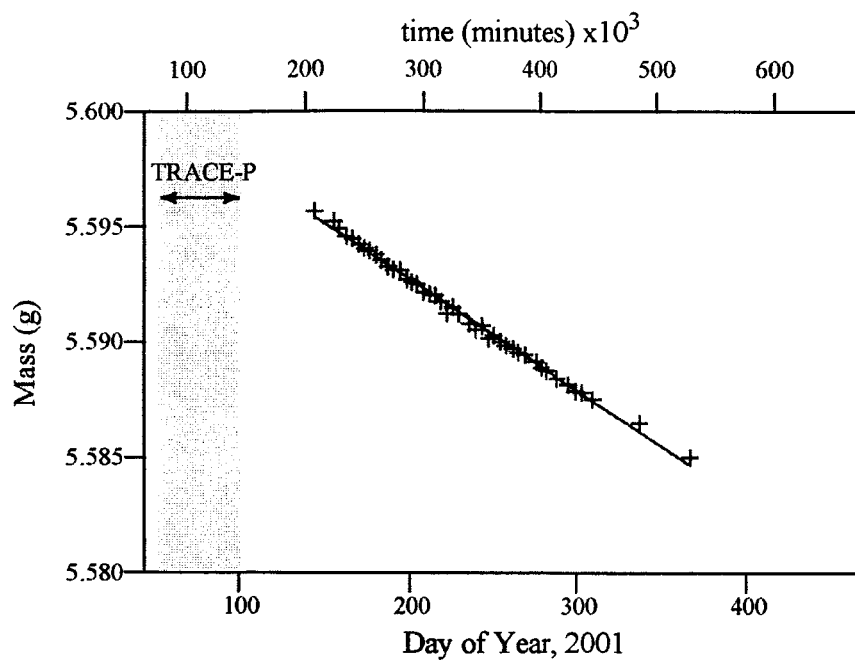


Figure 7. A plot of the mass of the H^{15}NO_3 permeation tube as a function of time. A linear regression of the data ($\pm 2\sigma$) yielded a slope of $-33.5 \pm 1.3 \text{ ng min}^{-1}$ and an intercept of $5.6024 \pm 0.0004 \text{ g}$ for a 7+ month period after TRACE-P.

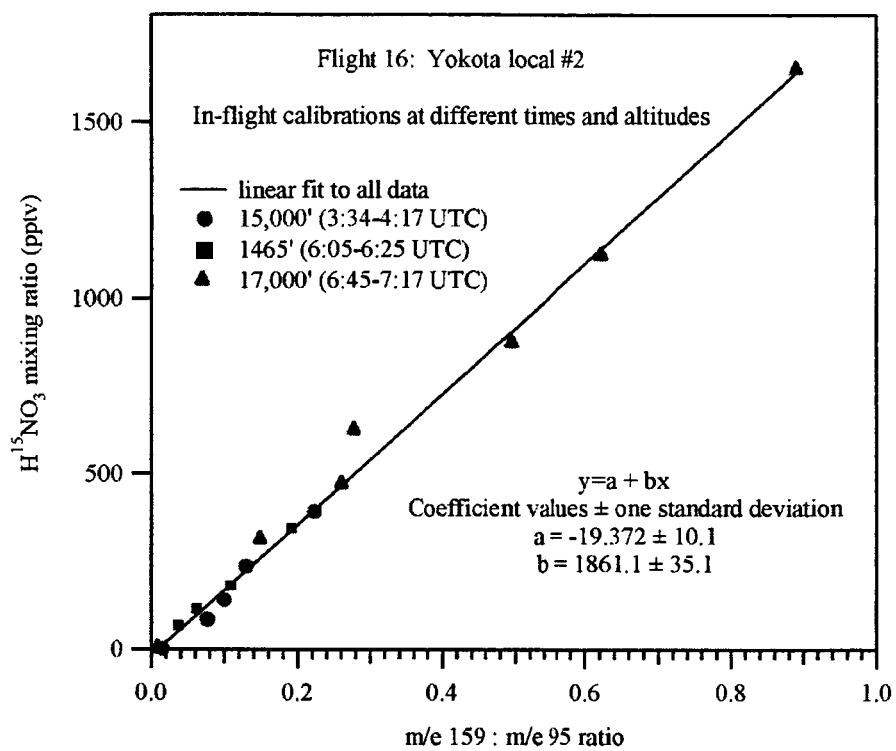


Figure 8. Plot of in-flight calibrations taken at multiple altitudes during Flight 16. The calibrations were conducted at constant altitude legs by adjusting the dilution of calibration gas.

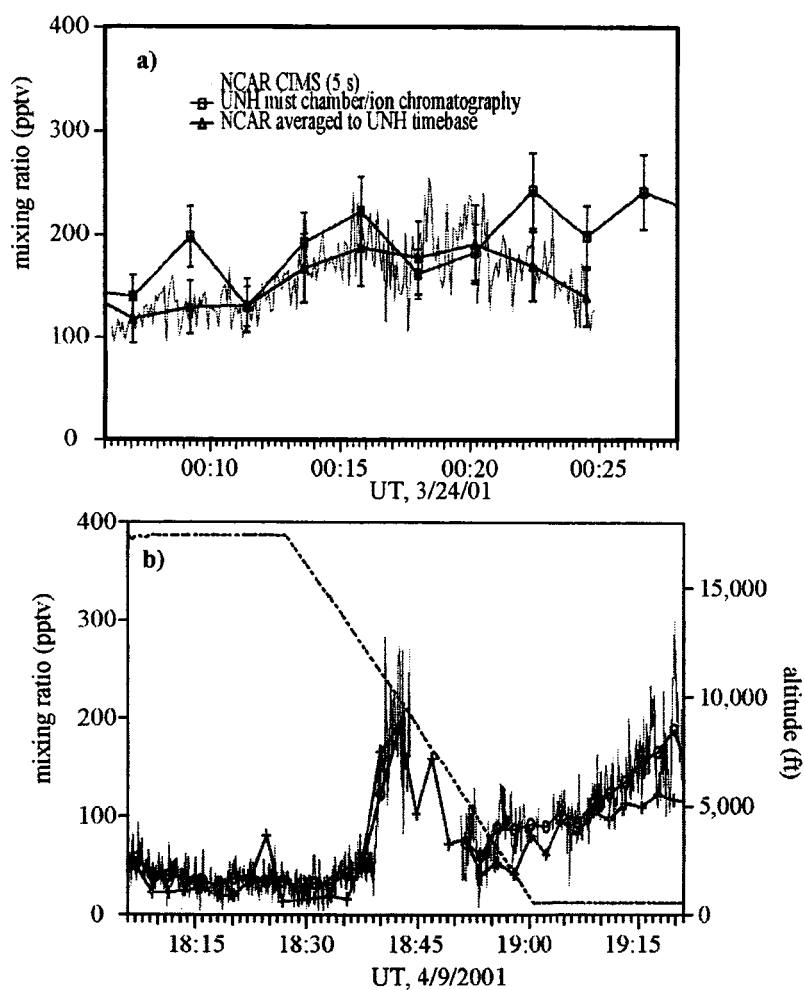


Figure 9. Results of the informal intercomparisons for HNO₃ on (a) DC-8 flight #10 and P-3B flight #16 at 17,000' off the Japan coast as well as (b) DC-8 flight #20 and P-3B flight #23 at a range of altitudes just east of Hawaii. The light blue, thin lines are the 5 s data obtained from the NCAR CIMS instrument. The red crosses are the HNO₃ mixing ratios measured on the DC-8 from the UNH mist chamber/ion chromatograph instrument. The dark blue circles are the NCAR data averaged over the UNH time base.

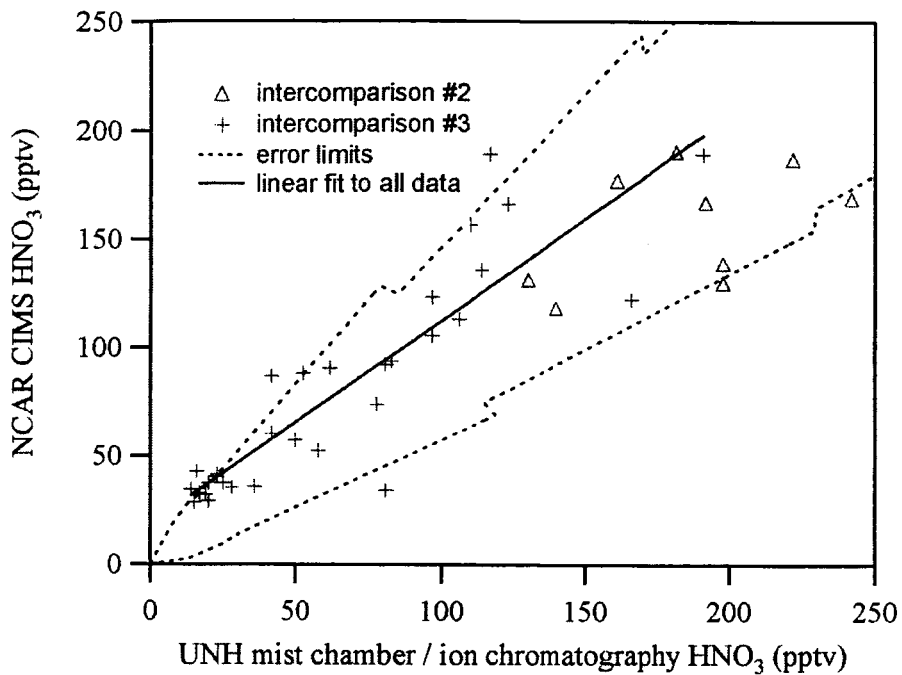


Figure 10. A plot of NCAR HNO₃ vs. UNH HNO₃ for the intercomparison flights. Triangles show intercomparison #2 while crosses mark intercomparison #3. A linear fit to the data yields an intercept of 19 ± 14 and a slope of 0.94 ± 0.18 (2σ). Dashed lines show the error limits of the two measurement.

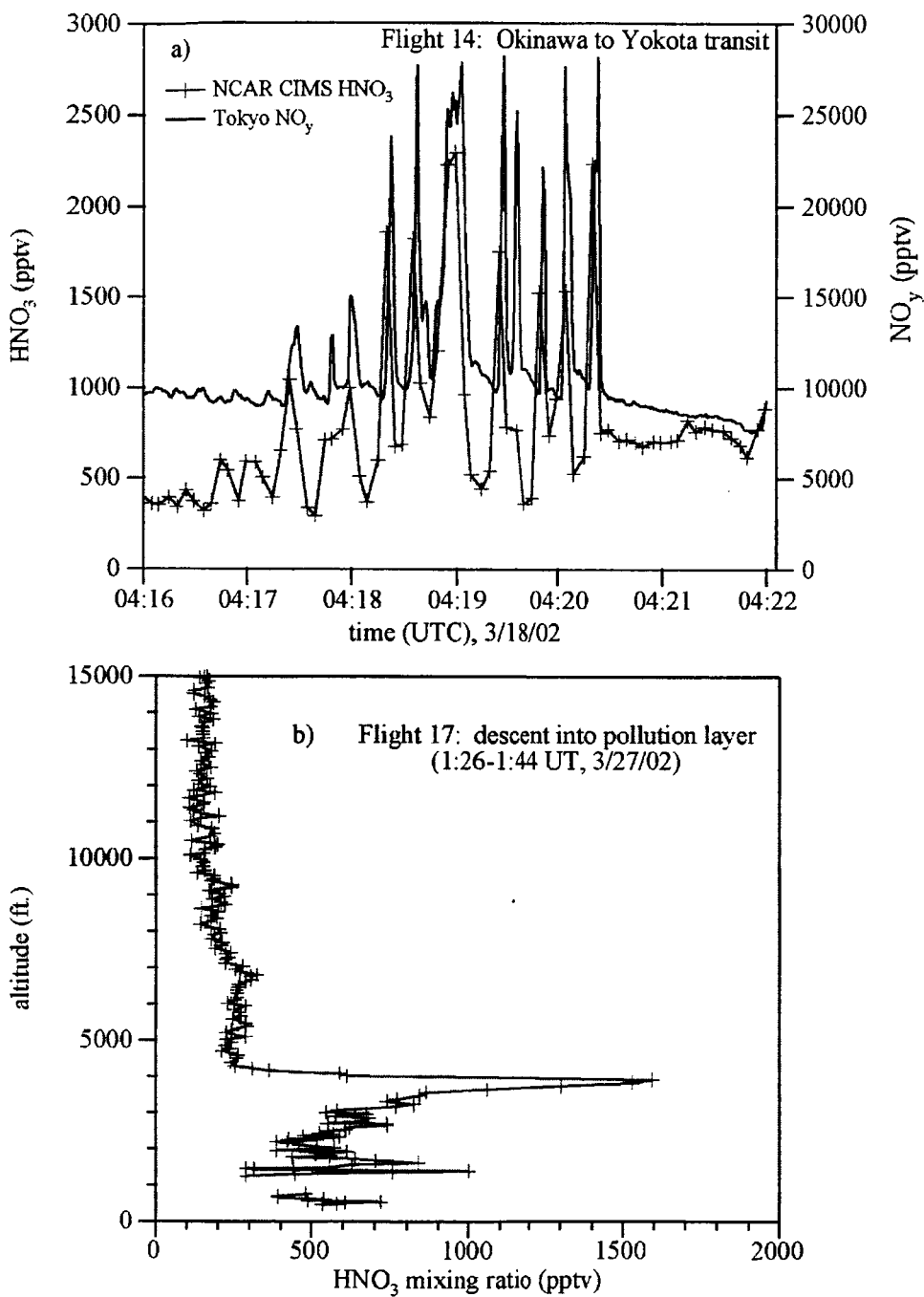


Figure 11. Rapid changes in ambient HNO₃ were observed during TRACE-P, suggesting that inlet adsorption problems were not significantly affecting the measurements. a) Ship plumes over the South China Sea at 500' showing rapid variations on the 5 s measurement time b) Descent into pollution southeast of Japan showing a greater than 1200 pptv increase in 15 s.